AD-769 800

BROADBAND ANTENNA SYSTEMS REALIZED
FROM ACTIVE CIRCUIT CONJUGATE IMPEDANCE
MATCHING

Albert Kevin Perry

Naval Postgraduate School
Monterey, California

September 1973

NAVAL POSTGRADUATE SCHOOL
Monterey, California

THESIS

BROADBAND ANTENNA SYSTEMS REALIZED
from
ACTIVE CIRCUIT CONJUGATE IMPEDANCE MATCHING

by

ALBERT KEVIN PERRY

Thesis Advisor: Paul E. Cooper

September 1973

Approved for public release; distribution unlimited.

REPORT DOCUMENTATION PAGE		READ INSTRUCTIONS BEFORE COMPLETING FORM
1. REPORT NUMBER	2. GOVT ACCESSION NO.	3. RECIPIENT'S CATALOG NUMBER
4. TITLE (and Subtitle) BROADBAND ANTENNA SYSTEMS REALIZED FROM ACTIVE CIRCUIT CONJUGATE IMPEDANCE MATCHING		5. TYPE OF REPORT & PERIOD COVERED Electrical Engineer's Degree; September 1973
		6. PERFORMING ORG. REPORT NUMBER
7. AUTHOR(s) Albert Kevin Perry		8. CONTRACT OR GRANT NUMBER(s)
9. PERFORMING ORGANIZATION NAME AND ADDRESS Naval Postgraduate School Monterey, California 93940		10. PROGRAM ELEMENT, PROJECT, TASK AREA & WORK UNIT NUMBERS
11. CONTROLLING OFFICE NAME AND ADDRESS Naval Postgraduate School Monterey, California 93940		12. REPORT DATE September 1973
		13. NUMBER OF PAGES 92
14. MONITORING AGENCY NAME & ADDRESS(If different from Controlling Office) Naval Postgraduate School Monterey, California 93940		15. SECURITY CLASS. (of this report) Unclassified
		15a. DECLASSIFICATION/DOWNGRADING SCHEDULE

16. DISTRIBUTION STATEMENT (of this Report)

Approved for public release; distribution unlimited.

17. DISTRIBUTION STATEMENT (of the abstract entered in Block 20, if different from Report)

18. SUPPLEMENTARY NOTES

19. KEY WORDS (Continue on reverse side if necessary and identify by block number)

broadband antenna systems, negative impedance, conjugate impedance matching, active circuit matching, negative capacitance

20. ABSTRACT (Continue on reverse side if necessary and identify by block number)

The application of negative impedance converter circuits for use in extremely broadband antenna systems is proposed. The theory of short antennaes, and means of achieving a conjugate impedance match to them, is discussed. Synthesis methods that yield the required converters, uncompensated or compensated, are presented. Lastly, the performance of several of the constructed antenna systems are compared with that of a 12 foot whip.

BROADBAND ANTENNA SYSTEMS REALIZED
from
ACTIVE CIRCUIT CONJUGATE IMPEDANCE MATCHING

by

ALBERT KEVIN PERRY
Lieutenant, United States Navy
B.S., University of Michigan, 1966

Submitted in partial fulfillment of the
requirements for the degree of

ELECTRICAL ENGINEER

from the

NAVAL POSTGRADUATE SCHOOL
September 1973

Author _____

Approved by: _____
Thesis Advisor

_____
Second Reader

_____
Chairman, Department of Electrical Engineering

_____
Academic Dean

ABSTRACT

The application of negative impedance converter circuits for use in extremely broadband antenna systems is proposed. The theory of short antennaes, and means of achieving a conjugate impedance match to them, is discussed. Synthesis methods that yield the required converters, uncompensated or compensated, are presented. Lastly, the performance of several of the constructed antenna systems are compared with that of a 12 foot whip.

TABLE OF CONTENTS

I. INTRODUCTION

Conjugate impedance matching is a potentially powerful method for obtaining broadband signal reception from short antenna systems. By employing active element networks, it is theoretically possible to modify the characteristics of a given antenna so as to make it essentially resonant over extremely large frequency ranges. Not unexpectedly, the exact loading that the active network is required to present to the antenna is a function of the shape, size, and frequency of operation at which the antenna probe is being used.

In essence, the technique is to reduce, by active matching, the impedance of the receiving probe to a purely resistive value over an extended frequency range, hence achieving the broadband resonance effect. In the conventional sense, inductors and/or capacitors are matched to the antenna to provide single frequency resonance. Likewise, in the active antenna system, to achieve the resonance characteristics desired, the conjugate match of the antenna impedance is synthesized by use of active networks and then presented to the antenna. The result of such manipulations is the obtainment of high Q, yet broadband, reception systems where the common antenna size versus wavelength relationships do not apply.

A. BACKGROUND

The concept of using loading to cause antenna resonance dates back to the turn of the century, when it was common practice to use inductors and capacitors to tune or detune antenna structures. The problem of matching antennaes using passive networks, based on numerous matching criterias, has been treated extensively by various authors [Ref. 1 and 2].

Conjugate impedance matching functions accomplished by means of active networks have received only minimal attention. Early work in this field was done by Merrill [Ref. 3] and Bonner [Ref. 4]. Recently, McMahon [Ref. 5] has attempted to use active conjugate impedance matching methods in order to obtain broadband control of radar cross sections. With regard to antenna systems, only two published works have appeared. The first, by Mittra [Ref. 6], is extremely restrictive in nature. The second, an investigation of one possible broadband antenna system, was reported in Reference 7.

Hence, out of necessity, experimental work had to progress, for purposes of this report, along two separate lines: circuit development and matching to the selected antenna form.

B. REPORT FORMAT

Chapter two presents the theory of broadband antenna conjugate matching. Chapter three deals with the experimental methods used in testing the realized devices and systems. Chapter four summarizes the device construction procedures and the experimental results obtained, while chapter five presents the conclusions.

II. BROADBAND ANTENNA CONJUGATE IMPEDANCE MATCHING THEORY

The following sections present the theory behind the concept of the broadband resonant antenna. Small antenna theory is briefly reviewed, and then extended to allow for broadband resonance by introducing the concept of the negative reactance element. Means of achieving such negative elements are formulated, and then the overall result is applied to the development of antenna matching schemes that yield the desired broadband resonance phenomenon.

A. SMALL ANTENNA THEORY

For purposes of definition, the short antenna is defined as one whose dimensions are much smaller than the wavelength of interest. Such a short receiving antenna can be modeled by a Thevenin generator having a voltage V_s and an internal antenna impedance Z_a as shown in Figure 1.
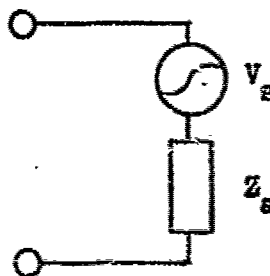

Fig. 1. Short Antenna Equivalent Circuit

1. Antenna Impedance

Z_a is generally complex and composed of a resistance component R_a and a reactive component X_a.

Given a short antenna of length L and radius a, where L is much less than $\lambda/4$, the input reactance of the antenna structure is capacitive, and given by the approximation

$$C_s \approx \frac{2\pi e_o L}{[\ln(L/a)-1]}.$$

If, in addition, capacitive top loading is employed to increase the effective height of the antenna and provide an essentially uniform current distribution, a second capacitance, top loading capacitance, C_t, must be accounted for in X_a. Such top capacitance is effectively added in parallel with the structure capacitance C_s. For computational purposes, C_t is a linear function of the diameter of the geometric form employed and is shown by the curves of Figure 2 [Ref. 8].
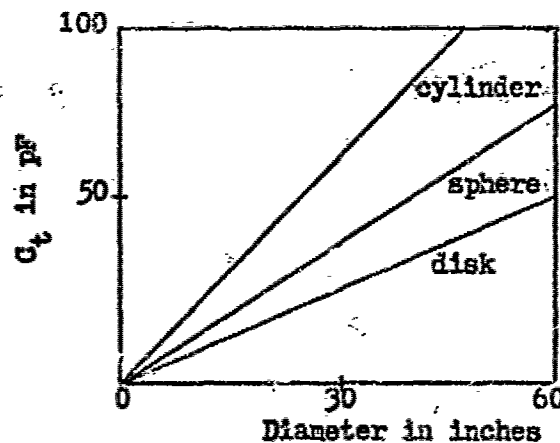
Fig. 2. Top-loading Capacitance of Various Geometric Forms
vs Their Diameter

The antenna resistance is composed of two parts, the first of which is termed the radiation resistance, R_r. The radiation resistance for a short antenna with an essentially uniform current distribution can be shown to be approximately twice that of a structure having linear current distribution, and is given by

$$R_r = 80\pi^2 (L/\lambda)^2.$$

When considered over a perfect ground plane, this resistive component is again doubled and thus equivalent to

$$R_{r_{over ground}} \approx 1600 (L/\lambda)^2.$$

8

A second resistance, R_1, the ohmic loss resistance, is also present, but since it is usually much less than the radiation resistance, it is neglected in future considerations.

Returning to Figure 1, we may model the short, capacitively top loaded antenna by either of the following equivalent circuits,
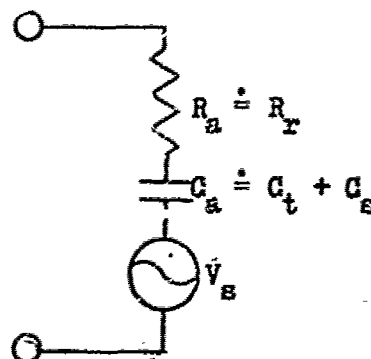
Fig. 3a. Thevenin Antenna Equivalent Circuit   Fig. 3b. Norton Antenna Equivalent Circuit
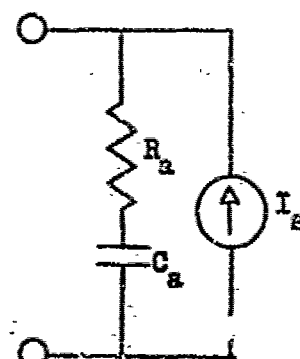
where V_s and I_s represent the respective voltage or current impressed on the antenna at some frequency f_1.

B. SINGLE FREQUENCY IMPEDANCE MATCHING

Consider the resultant Thevenin's equivalent antenna circuit given above. The conventional impedance matching approach for achieving maximum signal reception is to reduce the net antenna reactance to zero by introducing a series inductance so as to obtain resonance at the desired frequency. At the resonant frequency, f_r, the antenna input impedance reduces to R_r, a minimal impedance value, and the current is maximized. Graphically, the above is presented in the following:

9

$X_L = \omega L$

$Z = \sqrt{R^2 + X^2}$

Impedance

R

f

f_r

$X_C = -1/\omega C$

L

R_a

C_a

V_S
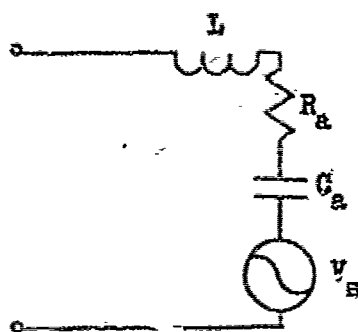
Fig. 4a. Inductively Tuned Antenna Model
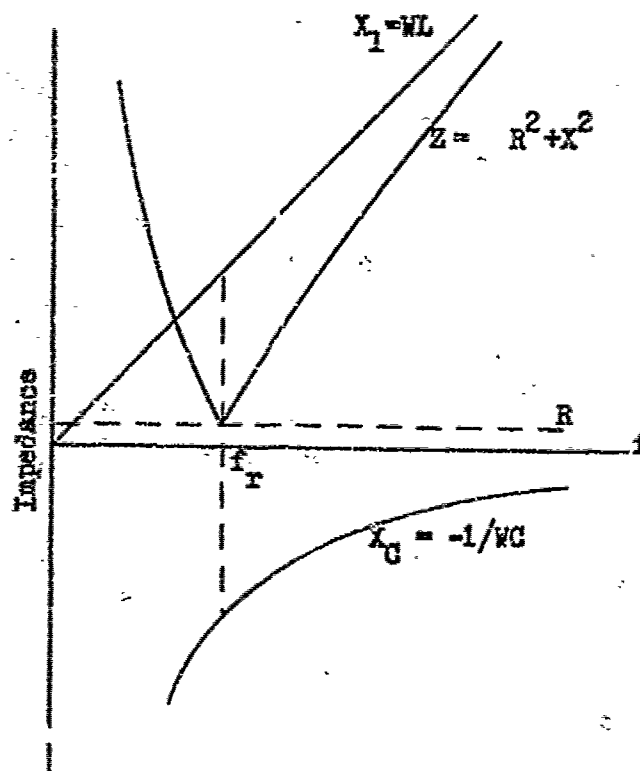
Fig. 4b. Impedance vs Frequency Plot for Inductively Tuned, Capacitive Antenna

The major drawback of this method is, of course, that resonance with inherently high Q is obtained at only one frequency, f_r. This failing is effectively removed if one hypothesizes the existence of a negative capacitance, $-C_b$. If $C_a = -C_b$, and the negative element was substituted for the inductance shown in Figure 4a, it becomes readily apparent that the antenna would be resonant and present an impedance $Z_a = R_r$ at all frequencies. For continuity, we digress at this point to consider the significance of such a negative element.

C. NEGATIVE CAPACITANCE

An idealized model of a negative capacitance, shown in Figure 5,
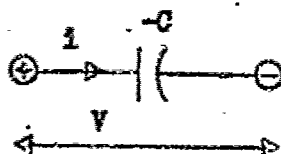
Fig. 5. Idealized Negative Capacitor Model

is an active element that can mathematically be described by,

$$i(t) = -C \, dv/dt, \qquad (1)$$

or equivalently,

$$v(t) = (1/-C) \int i(t) \, dt , \qquad (2)$$

In both of the above, the minus sign is implicitly assumed to be associated to the element C, vice a current reversal or negative voltage-time gradient.

A combination of series capacitors, one positive, the other negative, results in an equivalent short circuit, as shown in the following:
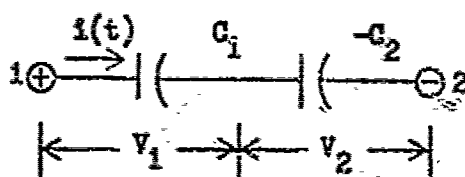
Fig. 6. Series Capacitor Placement Model

Between the terminals 1-2,

$$\frac{1}{C_t} \int i(t) \, dt = \frac{1}{C_1} \int i(t) \, dt + \frac{1}{-C_2} \int i(t) \, dt ,$$

$$\frac{1}{C_t} = \frac{1}{C_1} + \frac{1}{-C_2} ,$$

$$C_t = -C_1 C_2 / (C_1 - C_2) .$$

For $C_1 = |-C_2|$, C_t goes to infinity, which in idealized form is the equivalent of an electrical short.

11

Shunting parallel capacitors, one positive, the other negative, as shown in Figure 7, results in an open.
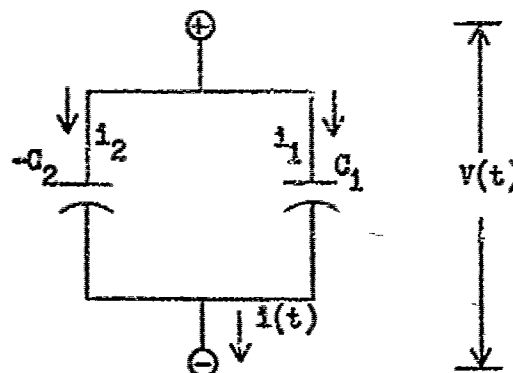
Fig. 7. Parallel Capacitor Placement Model

Between the terminals 1-2,

$$C_t \frac{dv(t)}{dt} = C_1 \frac{dv(t)}{dt} - C_2 \frac{dv(t)}{dt} \quad ,$$

$$C_t = C_1 - C_2 \quad ,$$

For $C_1 = |-C_2|$, $\qquad C_t = 0$.

Finally, in terms of the frequency domain,

$$C_1 \rightarrow -j/wC_1, \quad -C_2 \rightarrow j/wC_2 .$$

By analogy of form, the negative capacitor acts as an inductor of value $1/C_2$, with the same current-voltage-phase relations, but with the important difference that the frequency dependence is the inverse.

1. <u>Series Placement</u>

Consider the series form shown in Figure 8. For purposes of
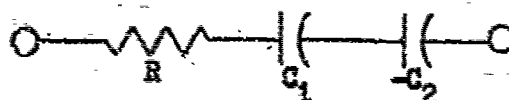
Fig. 8. Series R, C_1 -C_2 Placement

analysis, R is considered to be the lumped series leg resistance, and C_1 is by assumption equal to $|-C_2|$. Thus,

$$Z = R - j/wC_1 + j/wC_2 \qquad (3)$$

$$Z = R$$

The voltage and current are in phase, $Z(s)$ is minimum, and $I(s)$ is maximum. The impedance vs frequency plot is given by the following:
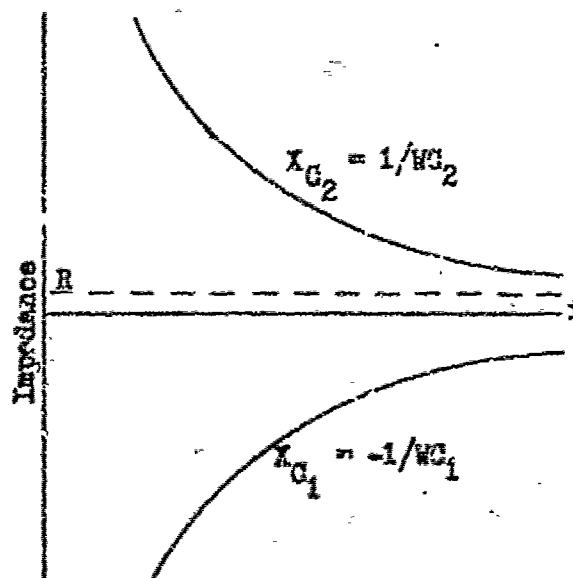
Fig. 9. Impedance vs Frequency Plot for Series Placed Negative Capacitor

If conventional Q definitions are used, then

$$Q = \frac{2\pi \text{ maximum stored energy}}{\text{energy dissipated per cycle}} , \qquad (4)$$

$$Q = \frac{1}{wCR} , \qquad (5)$$

A proof of this result is presented below; for now though, consider that since the sum of the reactance parts is zero at all frequencies, Q does not peak in the conventional sense, but exhibits a characteristic behaviour as shown in Figure 10.

13
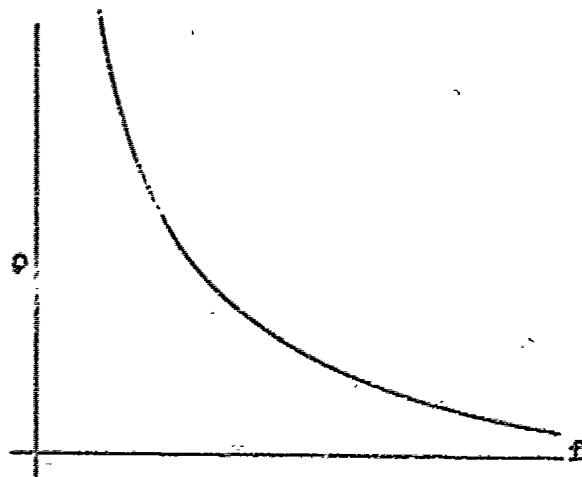
Fig. 10. Q vs Frequency for Element Placement of
Figure 8

For short, top loaded antennas with typical parameters,
$C_t \approx 2$ pF, $R \approx .1$ ohms, Q would range from $5 \cdot 10^{10}$ at KHz, to $5 \cdot 10^5$ at
1 GHz.

At any given frequency f_i, the energy stored is a constant, but
different than the amount present at frequency f_j. In terms of the ac-
tive and reactive power, the external circuit is not called upon to fur-
nish any reactive power to the resonant circuit. The reactive power is
transferring energy back and forth from the negative capacitor to the
positive capacitor within the resonant circuit. Hence, the terminal volt-
age and current are in phase; their product is a minimum at any frequency;
their power factor is unity. These conclusions are evident from consid-
ering a current $i(t) = I_m \sin \omega t$ passing through the series elements of
figure 8. The voltage V_{C_1} across the positive capacitor alone is given
by:

$$V_{C_1} = \frac{-I_m \cos \omega t}{\omega C} ,$$ (6)

14

while that across the negative capacitor is:

$$V_{C_2} = \frac{I_m \cos wt}{wC} .$$ (7)

The phase, current, and voltage relations that exist across $-C_2$ are identical to those of an inductor. In particular, when the positive capacitor voltage is a maximum, the current through the negative capacitor is zero, and vice versa. For an inductor, $V_1 = wLI_m \cos wt$, while V_{-C_2} equates to equation 7. By analogy, $L = 1/(w^2 |C_2|)$, hence, the energy stored in the negative capacitor, $-C_2$, is

$$E_{-C_2} = \left(\frac{1}{2} \frac{1}{w^2 |C_2|} \right) I_{max}^2 \sin^2 wt ,$$

while that in the positive capacitor is

$$E_{C_1} = \left(\frac{1}{2} \frac{1}{w^2 C_1} \right) I_{max}^2 \cos^2 wt \qquad .$$

Therefore, the total stored energy in the system at any moment is given by:

$$
\begin{aligned}
E_{stored} &= E_{C_1} + E_{-C_2} \\
&= \frac{1}{2} \frac{I_{max}^2}{w^2 C_1} \left[\cos^2 wt + \sin^2 wt \right] \\
&= \frac{1}{2} \frac{I_{max}^2}{w^2 C_1} \qquad \text{for } C_1 = |-C_2| .
\end{aligned}
$$

At the instant of maximum current, all energy is stored in the negative capacitor; at the instant of zero current, all the energy is stored in the positive capacitor. Thus, since the sum of the cosine-squared, sine-squared, functions is always unity, the total stored energy is a constant independent of time.

15

The energy dissipated per cycle is given by $\frac{1}{2}I_m^2 R/f$, thus from the previously stated definition for Q,

$$Q = \frac{2\pi\left(\frac{1}{2}I_{max}^2/w^2 C_1\right)}{\left(\frac{1}{2}I_{max}^2 R/f\right)} = \frac{1}{wC_1 R} ,$$

which is the same as was given in equation 5.

2. Parallel Placement

Consideration is now given to the parallel circuit form of Figure 11. This is identical to Figure 3b, with the exception that an element of value $-C_2$ has been placed in shunt across the terminals.
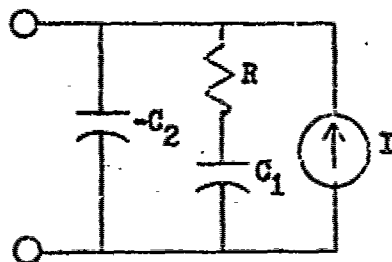
Fig. 11. Shunt Placed Negative Capacitor

Analysis of this circuit yields:

$$Y = \frac{1}{R + \frac{1}{jwC_1}} - jwC_2 ,$$

$$Y = \frac{jwC_1(1-jRwC_1)}{R^2 w^2 C_1^2 + 1} - jwC_2 ,$$

$$Y = \frac{Rw^2 C_1^2}{R^2 w^2 C_1^2 + 1} + \frac{jwC_1}{R^2 w^2 C_1^2 + 1} - jwC_2 .$$

For frequencies less than several hundred MHz, $R^2 w^2 C_1^2$ is much less than one, so that the above reduces to:

$$Y \doteq Rw^2C_1^2 + j(wC_1 - wC_2) \qquad ,$$

$$Y \doteq w^2C_1^2 \left[R + j(\frac{1}{wC_1} - \frac{-1}{wC_2}) \right] , \text{ where } C_1 = |-C_2| . \quad (8)$$

Equation 8 is of the same form as equation 3. Therefore, Y for the parallel circuit varies with frequency in a manner similar to that for Z of the series circuit of Figure 9. The susceptance vs frequency plot is given in Figure 12. Of particular interest is the conductance
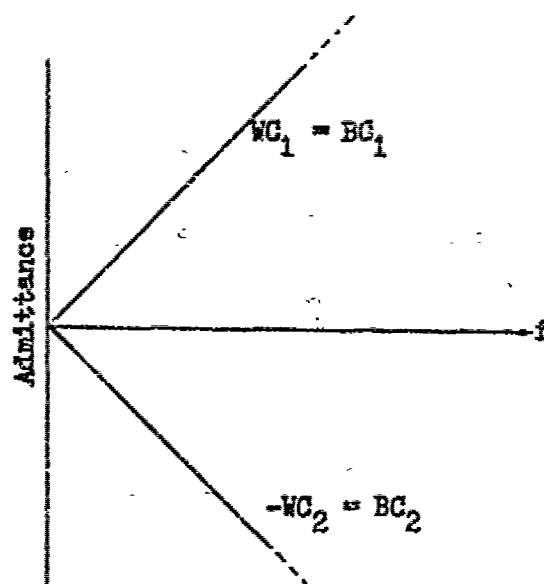
Fig. 12. Susceptance vs Frequency for Shunted Negative Capacitor Placement

presented by this circuit arrangement, which is now considered. From equation 8, Z is given by:

$$Z = 1/w^2C_1^2R . \qquad (9)$$

This is more conveniently expressed in terms of Q. Using the previously given definition for Q, the value for the two branch parallel resonant circuit is:

$$Q = 1/wC_1R , \qquad (10)$$

17

which is the same Q as found for the series circuit. Thus, Q will vary as shown in Figure 13. Substituting equation 9 in to 10 yields the result:

$$Z = Q^2 R \ .$$

Thus, at resonance, the parallel tank presents an input resistance that varies as plotted in Figure 13.
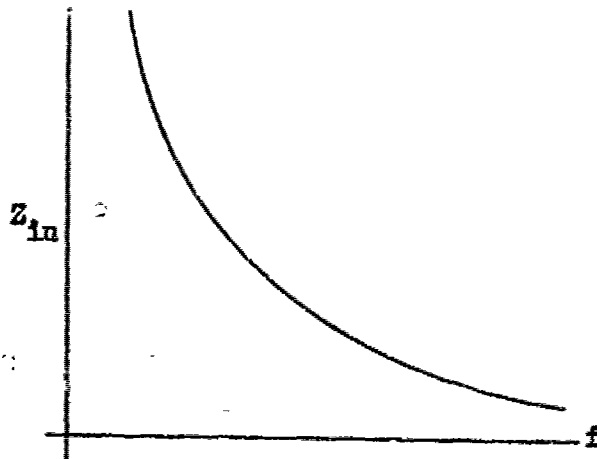
Fig. 13. Input Impedance vs Frequency for Parallel Element Placement of Figure 11.

The preceding discussion of the parallel placement model assumes all the resistance present in the circuit to be in the branch leg containing the antenna, with none in the negative capacitor shunt branch. This may not actually be the case. Resistance may be present in either of the two branches. Whatever the case, all resistance placements require high Q to be valid, and so long as the Q is high, it makes little difference how the resistance is distributed. True, the above formulations would vary, but as in a LC tank, they would still serve as excellent approximations. Hence, for R small, R is considered to be the sum of the resistances present in each branch leg.

From the above treatment of the series and parallel circuit models, it is evident that broadband, high Q, matching is possible by

the use of negative capacitance elements. Our next consideration is to the approximate realization of such an element.

D. NEGATIVE IMPEDANCE CONVERTER THEORY

The means by which the negative capacitance discussed in the previous section is to be obtained is by the use of Negative Impedance Converters, (NIC). Since Linvill published his original paper on active filter synthesis in 1953, and introduced the first practical transistorized NIC, the concept of active converter circuits has become accepted. Though the actual credit for the concept of negative impedance converters is generally credited to Marius Latour for his work on negative regenerative systems, little actual use for the device or theory was made until the field of active filters became established.

The functional aspects of NIC's are today well documented for the idealized form; hence, the following discussion serves only to provide an introductory medium for later discussion.

1. General NIC Theory

A negative impedance converter is by definition a two port device with the property that any immittance shunted across one terminal pair will appear as the negative of that immittance at the other port. It is, by analogy, a form of an ideal transformer; it has a ratio of impedance transformation of $-K$:1 and functions in a bilateral manner [Ref. 9].

A concise definition of the properties of an NIC may be arrived at by consideration of the terminal voltages and currents of a two port. For convenience, the two port is described by its hybrid parameters as shown in Figure 14.

19
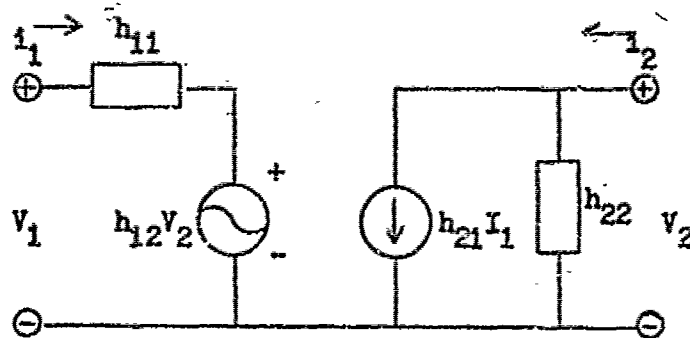
Fig. 14. H Parameter Two Port Model

The conventional parameter designations apply and are related by:

$$V_1 = h_{11}I_1 + h_{12}V_2 \;,$$

$$I_2 = h_{21}I_1 + h_{22}V_2 \;.$$

If in the above figure a load impedance Z_1 is placed across port 2, Z_{in} may be expressed as:

$$Z_{in} = V_1/I_1 = h_{11} - \frac{h_{12}h_{21}Z_1}{1+h_{22}Z_1} \;,$$

where the product $h_{12}h_{21}$ is normally denoted by K and referred to as the devices conversion ratio, or equivalently, the devices transmission gain.

For $Z_{in} = -Z_1$, it is required that the following set of equations be satisfied:

$$h_{11} = 0$$

$$h_{22} = 0$$

$$h_{12}h_{21} = 1 \;.$$

The fact that $h_{12}h_{21} = 1$ leads to the title of unity, or ideal, NIC. It will be assumed in this section that all references to NIC's emphatically imply devices with unity conversion ratio.

Two basic types of NICs are realizable from the set of equations given above, depending on whether current or voltage inversion occurs.

20

A NIC that inverts current, INIC, does so without effecting the polarity of the input and output voltages. By definition, if the two port NIC device somehow inverts one port current with respect to the normal current flow in a passive network, the NIC is of an INIC type. With a load Z_1 on port 2 of Figure 14, the inversion of one port current results in V_1 producing a current flow in an opposite direction such as to oppose the applied voltage. The input impedance is therefore negative, $V_1 = V_2$, and $I_1 = I_2$. In matrix form, this is given by

$$\begin{bmatrix} h_{11} & h_{12} \\ h_{21} & h_{22} \end{bmatrix} = \begin{bmatrix} 0 & 1 \\ 1 & 0 \end{bmatrix}. \quad \text{(INIC)} \qquad (11a)$$

The resultant INIC is representable as shown in Figure 15a.
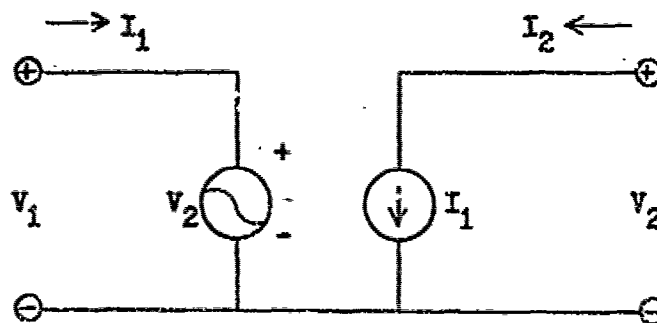
Fig. 15a. H Parameter Representation of INIC

When voltage is inverted, the direction of current flow through the NIC remains unchanged, and the device is referred to as a voltage inverter, or VNIC. For the ideal VNIC, $I_1 = -I_2$, and $V_1 = V_2$. In matrix form, this is expressible by:

$$\begin{bmatrix} h_{11} & h_{12} \\ h_{21} & h_{22} \end{bmatrix} = \begin{bmatrix} 0 & -1 \\ -1 & 0 \end{bmatrix}. \quad \text{(VNIC)} \qquad (11b)$$

21

The resultant VNIC model is given below.
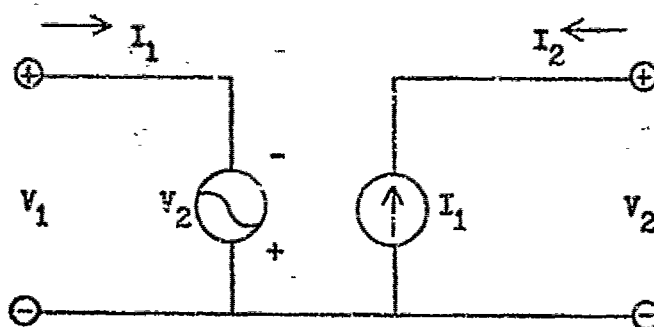
Fig. 15b. H Parameter Representation of VNIC

2. Circuit Realizability

Though the theory of NIC's is well established, synthesis pro-
cedures that allow for a concise developmental process for obtaining
circuit realizable forms have received minimal attention. Of the several
discrete NIC networks that have been developed over the last fifteen
years, almost all can be shown to reduce to the modelings of the ideal
representations shown in Figures 16 and 17.

$$h_{VNIC} = \begin{bmatrix} 0 & -1 \\ -1 & 0 \end{bmatrix} \Longleftrightarrow$$

Fig. 16a   Fig. 16b

$$H_{INIC} = \begin{bmatrix} 0 & 1 \\ 1 & 0 \end{bmatrix} \Longleftrightarrow$$
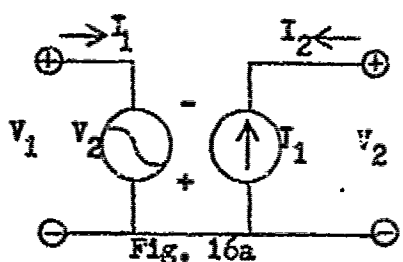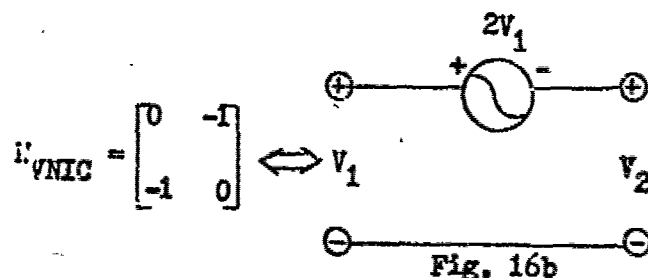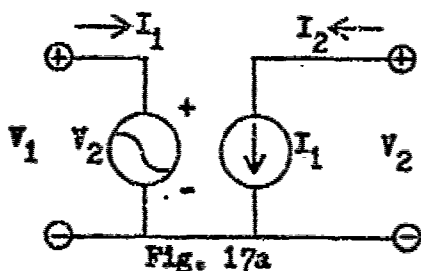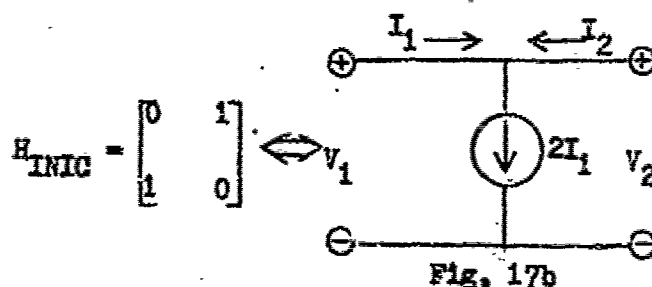
Fig. 17a   Fig. 17b

Concerning the above, the models on the left are most easily realized by the synthesis of a network to obtain the desired matrix form, while those on the right are constructed by approximating the desired current or voltage generators.

E. GENERATOR CONSTRUCTION

NIC circuits built on generator construction principles are inherently less complex than those based on matrix methods for the reason that it is easier to construct a dependent generator than to control two port matrix parameters. Two such generator models are now presented.

1. Idealized Generator VNIC Model

A particularly simple NIC circuit is given in Figure 18.
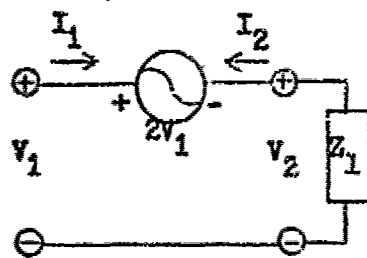
Fig. 18.   Idealized Generator
           VNIC Model
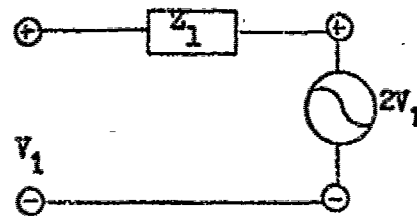
Fig. 19.   Modified Ideal Generator
           VNIC Model

For the above, $V_2 = -V_1$,

$$I_2 = -V_2/Z_1 = V_1/V_2 \qquad ,$$

$$\text{and } Z_{in} = V_1/I_1 = -V_1/I_2 = -Z_1 .$$

The modified arrangement of Figure 19 yields the same result, while being somewhat easier to realize by usage of amplifier stages as illustrated in Figure 20, where the input impedance of the amplifier stage is infinite, and $Z_{out} =$ zero.
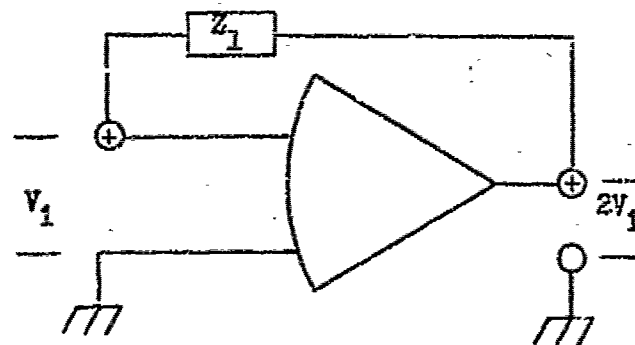
Fig. 20. Modified VNIC Configuration

This configuration readily lends itself to realization by use of high gain, differential, operational amplifiers as shown in Figure 21.
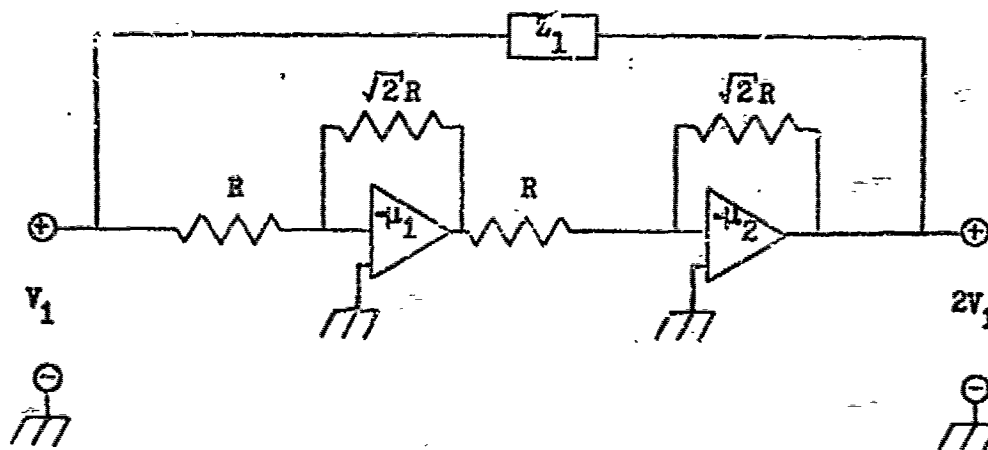
Fig. 21. VNIC Realization

In the above, the operational amplifiers are idealized as infinite input, zero output resistance, infinite gain stages.

The idealized operational amplifier is, of course, not available. It can be shown that as either finite input and output stage resistances develop, or as a phase shift arises with respect to the input and output voltages, the converter action deteriorates to an unusable point. Yet, at low frequencies, the above circuit is most practical when neither of the primary input-output terminals must be placed at ground potential.

2. Idealized Generator INIC Model

Figure 22 is a model representation of Figure 17a. Again,
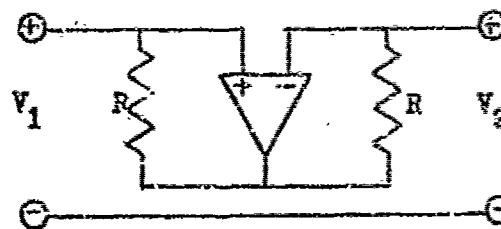
Fig. 22. Idealized Realization of INIC

assuming that the amplifier has high gain and infinite input impedance, there is a virtual short at the input terminals, which implies that $V_1 = V_2$. The two resistors thus have equal voltages across them, and since the amplifier draws no input current, $I_1 = I_2$, thus satisfying the conditions for INIC operation. As before, as the real operational amplifier configuration is approached, converter action degenerates, though at frequencies of operation less than 500 KHz, the above circuit is quite attractive.

3. General Generator Equivalent Circuits

A last comment is appropriate at this point. The generator equivalent NIC circuits are not true two port NIC's, only approximations, since they do not satisfy the stated matrix requirements; nevertheless, they are extremely useful when working with one port applications.

F. MATRIX FORMULATION

In the construction of the NIC's used in this report, two synthesis procedures were followed when possible. The first procedure is based on the principle that knowing the limitations under which a nonideal NIC may be compensated, one can construct a network that possesses matrix parameters that can be manipulated by matrix network synthesis

into an overall ideal NIC. The procedure developed for such compensation synthesis is covered separately, while in this section the active device arrangements that yield nonideal NIC's are discussed.

The second method considers the synthesis of NIC's from the nodal admittance matrix for the given network within which infinite gain amplifier stages have been inserted.

By utilizing the above design procedures, considerations such as frequency and dynamic range are, for the most part, reduced to considerations of the actual active devices employed.

1. Nonideal NIC Synthesis

In any matrix formed NIC circuit, a minimum of two active devices are required in order to make possible the feedback action necessary to produce negative impedance conversion. Hence, in its simplest form, the procedure for developing nonideal NIC's reduces to a study of the possible ways in which two active devices may be arranged while still presenting an H matrix for the network that can be synthesized into an ideal NIC "block." It will be shown in a later section that only those networks possessing an H matrix satisfying one of the entries of Table 1 may be compensated. Hence, it serves our purpose to consider only those active device arrangements that yield one of the entries listed in Table 1.

set	h_{11}	h_{22}	$h_{12}h_{21}$	Δh
1	≥ 0	≥ 0	> 0	≤ 0
2	≥ 0	≤ 0	> 0	≤ 0
3	≤ 0	≤ 0	> 0	≥ 0
4	≤ 0	≥ 0	> 0	≤ 0
5	≤ 0	≤ 0	> 0	≤ 0

Table 1. Compensatable NIC H Parameters

Assuming that the active devices are representable as three

terminal two ports, arranged as shown in Figure 23, then it can be
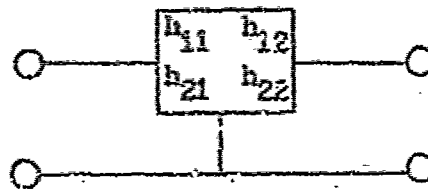
Fig. 23.   Active Device Three
Terminal Two Port

mathematically proven that the only interconnections that lead to re-

alizable, wideband NIC's are the series-parallel, parallel-series ar-

rangements depicted in Figures 24 and 25.[1]
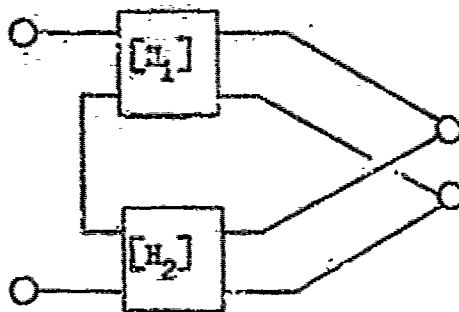
Fig. 24.   Series-Parallel NIC   Fig. 25.   Parallel-Series NIC
Configuration   Configuration
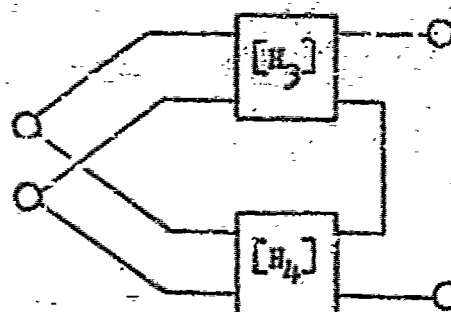
The series-series, parallel-parallel, and cascade configurations

are inferior due to the active device placement and associated biasing

problems, and/or excessive compensation required to realize the ideal

NIC conditions [Ref. 10].

---

[1]The main restriction is that the product $h_{12}h_{21}$ be positive in mag-
nitude. If one assumes active devices that are transistors, this implies
that only the common collector-common emitter, or vice versa, configura-
tions will have $h_{12}h_{21}$ products anywhere near unity. Given the device
arrangement of Figure 23, these arrangements reduce to the series-parallel,
or parallel-series forms above. For further examples, refer to "Handbook
of Semiconductor Electronics," 2nd edition, by L. Hunter, McGraw-Hill
publisher, p. 11-28 through 11-30.

The device employed in Figure 23 may be bipolar, fet, tube, or combinations thereof. Depending on the type of devices selected, Figures 24 and 25 would in some cases have to be modified to include external resistors inserted to prevent certain matrix elements from becoming infinite.

The most useful of the realizable configurations that can be derived from the above arrangements is given in Figure 26. The result-
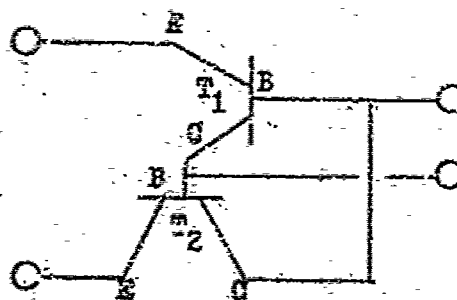
Fig. 26. Series-Parallel Realization
for Nonideal NIC

ant two port H matrix is given by equation 12, where the primes denote

$$(12) \quad [H_t] = \frac{1}{|\Delta h|^2} \begin{bmatrix} (h_{22}|\Delta h'| + |\Delta h'| h'_{22}) & -(h_{12}|\Delta h'| + h'_{21}|\Delta h|) \\ \\ -(h_{12}|\Delta h'| + h'_{21}|\Delta h|) & (h_{11}|\Delta h'| + h'_{22}|\Delta h|) \end{bmatrix}$$

parameters of the second device. The overall H matrix, $[H_t]$, is of interest since it presents the most favorable parameters for a non-ideal NIC; i.e., h_{11_t}, h_{22_t}, are very small, and h_{12_t}, h_{21_t}, are close to unity. Hence, the arrangement of Figure 26 will always provide a nonideal NIC, regardless of the conductance value inserted for biasing. It has been found that all other configurations derived from this procedure are, at best, only conditional nonideal NIC's. By this, is meant

that the conductance values of resistors used for biasing, and the parameter values of the active devices selected, must fall within certain restrictive ranges.

It is of interest to note that the arrangement given in Figure 26 is similar in form to the first transistorized NIC model proposed by Linvill [Ref. 11].

2. Nodal Admittance Synthesis

The procedure to be followed in this section is to synthesize out of a given nodal admittance matrix the conditions required for a two port to act as a negative impedance converter. Again, it is assumed that there are a minimum of two high gain amplifiers embedded within the two port. These active components, operational amplifiers for example, are considered to be three terminal, high gain devices with one terminal at ground potential. In general, the input impedance Z_{in} of Figure 27 can be expressed as a transformation of the load impedance Z_1 placed at
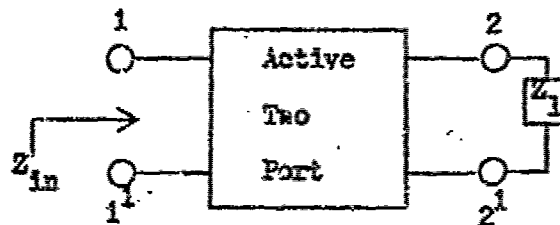
Fig. 27. Loaded, Active Two Port

port two:

$$Z_{in} = \frac{a + bZ_1}{c + dZ_1} , \tag{13}$$

where a through d are constants of the given network. It is assumed that the network is real and possesses a definite nodal admittance matrix, DNAM, of the form n x n, n > 2.

29

It has been shown by Holt and Carey [Ref. 12] in their paper on admittance transpose operations, that equation 13 can be rewritten in terms of the definite nodal admittance matrix so that,

$$Z_{in} = \frac{\Delta_{11} Z_1 + \Delta_{11,22}}{\Delta_{22} + \Delta \cdot Z_1} \quad . \tag{14}$$

In this equation, Δ_{ij} is the cofactor of the (i,j) element of the DNAM, Δ is the determinant, and $\Delta_{11,22}$ is the second order cofactor of the DNAM.

For Z_{in} to equal $-Z_1$, it is required that:

$$\Delta_{11,22} = \Delta = 0 \qquad , \tag{15a}$$

$$\frac{\Delta_{11}}{\Delta_{22}} = K = -1 = \text{conversion ratio.} \tag{15b}$$

From 15a,

$$\Delta = 0 \Rightarrow \Delta_{11} \Delta_{22} - \Delta_{12} \Delta_{21} = 0, \text{ or}$$

$$\Delta_{11} \Delta_{22} = \Delta_{12} \Delta_{21} . \tag{16}$$

Likewise, the voltage transfer ratio may be expressed as:

$$\frac{V_2}{V_1} = \frac{\Delta_{12} Z_1}{\Delta_{11} \cdot Z_1 + \Delta_{11,nn}} = \frac{\Delta_{12}}{\Delta_{11}} = N. \tag{17}$$

Thus, for a VNIC we would desire negative voltage gain, or $N = -1$. Combining equations 15 through 17, gives:

$$\Delta_{12} = -\Delta_{11} \qquad ,$$

$$\Delta_{11} = -\Delta_{22} \qquad ,$$

$$\Delta_{11} \Delta_{22} = \Delta_{12} \Delta_{21} \qquad ,$$

or, equivalently,

$$\Delta_{11} = -\Delta_{22} = -\Delta_{12} = \Delta_{21}. \quad [2] \tag{18}$$

Assume that it is desired to have one node of each input-output terminal pair at ground potential. Furthermore, for brevity, the gain stages are assumed not to be directly connected to the input or output terminals. Hence, there are a minimum of six nodes for each amplifier stage embedded, as depicted in Figure 28.
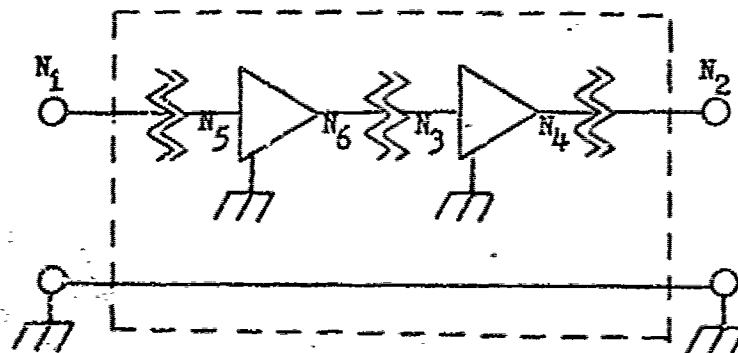
Fig. 28. Assumed Active Two Port Configuration

Since only two gain stages were specified, it is to be noted that any additional nodes would be composed of passive element junctions that could be removed by suppression techniques. In addition, because infinite gain stages are utilized, the input sides of each gain stage, nodes 3 and 5, must be at ground potential. Hence, V_3 and V_5 equal zero, and the resultant DNAM reduces to the fourth order form given below. g_{ij} is the conductance between nodes i and j, and the row/column index identify the specific terminal pairs.

---

[2] This derivation follows that of Reference 12, but extends the procedure to account for any arbitary load impedance Z_1.

	1	2	4	6
1	ε_{11}	$-\varepsilon_{12}$	$-\varepsilon_{14}$	$-\varepsilon_{16}$
2	$-\varepsilon_{21}$	$-\varepsilon_{22}$	$-\varepsilon_{24}$	$-\varepsilon_{26}$
3	$-\varepsilon_{31}$	$-\varepsilon_{32}$	$-\varepsilon_{34}$	$-\varepsilon_{36}$
5	$-\varepsilon_{51}$	$-\varepsilon_{52}$	$-\varepsilon_{54}$	$-\varepsilon_{56}$

The design procedure from this point on is based on two desires. First, synthesis yielding the minimum number of nonzero ε_{ij} elements, and secondly, satisfying the governing equations above, 15 through 18. From the DNAM,

$$\Delta_{11,\,22} = \varepsilon_{34}\varepsilon_{56} - \varepsilon_{36}\varepsilon_{54} = 0,$$

$$\text{or} \qquad \varepsilon_{34}\varepsilon_{56} = \varepsilon_{36}\varepsilon_{54} \qquad\qquad (19)$$

From equation 18,

$$-\Delta_{22} = \Delta_{21} = -\Delta_{12} = \Delta_{11} = \text{constant} \neq 0 \qquad,$$

where

$$\Delta_{11} = -\varepsilon_{22}(\varepsilon_{34}\varepsilon_{56} - \varepsilon_{36}\varepsilon_{54}) + \varepsilon_{32}(\varepsilon_{24}\varepsilon_{56} - \varepsilon_{26}\varepsilon_{54}) - \varepsilon_{52}(\varepsilon_{24}\varepsilon_{36} - \varepsilon_{26}\varepsilon_{34}),$$

$$\Delta_{12} = -\varepsilon_{21}(\varepsilon_{34}\varepsilon_{56} - \varepsilon_{36}\varepsilon_{54}) + \varepsilon_{31}(\varepsilon_{24}\varepsilon_{56} - \varepsilon_{26}\varepsilon_{54}) - \varepsilon_{51}(\varepsilon_{24}\varepsilon_{36} - \varepsilon_{34}\varepsilon_{26}),$$

$$\Delta_{21} = -\varepsilon_{12}(\varepsilon_{34}\varepsilon_{56} - \varepsilon_{36}\varepsilon_{54}) + \varepsilon_{32}(\varepsilon_{14}\varepsilon_{56} - \varepsilon_{16}\varepsilon_{54}) - \varepsilon_{52}(\varepsilon_{14}\varepsilon_{36} - \varepsilon_{16}\varepsilon_{34}),$$

$$\Delta_{22} = \varepsilon_{11}(\varepsilon_{34}\varepsilon_{56} - \varepsilon_{36}\varepsilon_{54}) + \varepsilon_{31}(\varepsilon_{14}\varepsilon_{56} - \varepsilon_{16}\varepsilon_{54}) - \varepsilon_{51}(\varepsilon_{14}\varepsilon_{36} - \varepsilon_{16}\varepsilon_{34}).$$

To satisfy equation 18, ε_{ij} terms are arbitarily set to zero. For example, setting

$$\varepsilon_{12} = \varepsilon_{14} = \varepsilon_{26} = \varepsilon_{13} = \varepsilon_{23} = \varepsilon_{56} = \varepsilon_{36} = \varepsilon_{21} = 0$$

yields

$$\Delta_{22} = \varepsilon_{51}(\varepsilon_{34}\varepsilon_{16}) = +0 \qquad,$$

$$\Delta_{21} = -g_{52}(g_{34}g_{16}) = -C ,$$

$$\Delta_{12} = g_{51}(g_{36}g_{24}) = +C ,$$

$$\Delta_{11} = -g_{52}(g_{36}g_{24}) = -C ,$$

hence,

$$g_{36}g_{24} = g_{34}g_{16} \tag{20}$$

$$g_{52} = g_{51} . \tag{21}$$

The resultant matrix is thus,

	1	2	4	6
1	g_{11}	0	0	$-g_{15}$
2	0	g_{22}	$-g_{24}$	0
3	0	0	$-g_{34}$	$-g_{36}$
5	$-g_{51}$	$-g_{52}$	0	0

where $\Delta = g_{15}g_{16}g_{24}(g_{34}-g_{36}).$

From equation 15, $\Delta = 0$, or equivalently, $g_{34} = g_{36}$. Lastly, for dominance, $g_{11} = g_{22}$; equations 19 and 20 yield $g_{16} = g_{24}$. Thus, in summary:

$$g_{52} = g_{51} = g_1$$

$$g_{34} = g_{36} = g_2$$

$$g_{16} = g_{24} = g_3 ,$$

and $\Delta_{11} = -\Delta_{22} = -\Delta_{12} = \Delta_{21}$ as required. Returning to Figure 28 and placing the resultant conductances in their respective places, yields Figure 29.
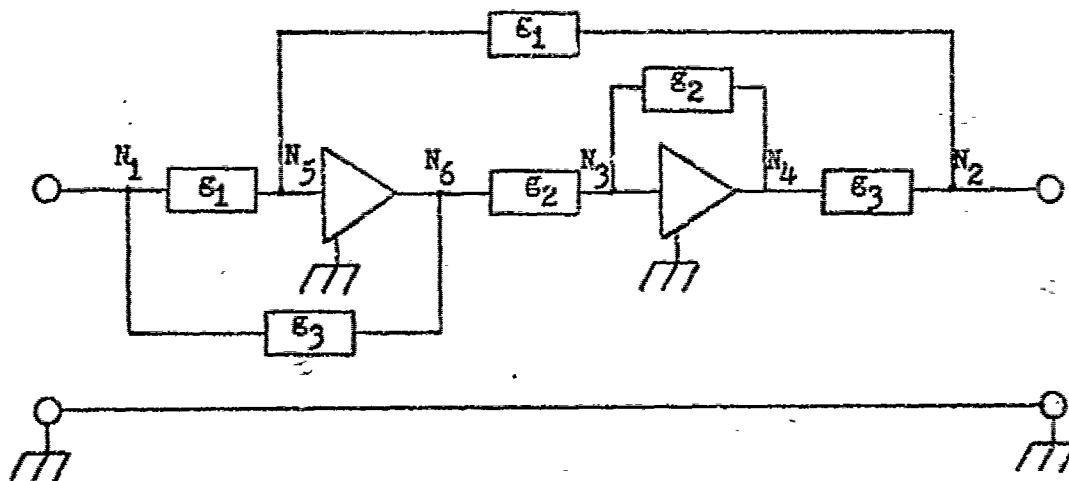
Fig. 29. Circuit VNIC Realization Based on Nodal Admittance Matrix

The resultant network is a VNIC, since it was required that $N=-1$. Reversing the amplifier setup results in a CNIC. It is of interest to note that the CNIC model was published by A. Antoniou [Ref. 13] and derived from his considerations of the circuits nonideal matrix form.

The circuit realization above is one of many that can be synthesized from the stated conditions. The main usefulness of this method is that desired configuration requirements are accounted for from the outset. Hence, terminal ground arrangements that would be difficult to achieve using other synthesis means, are handled in a relatively simple manner.

G. NONIDEAL COMPENSATION THEORY

In the ideal NIG, the immittance parameters h_{11} and h_{22} are both zero. For a nonideal NIC, the normally encountered situation, h_{11} and/or h_{22} are seldom zero. These resultant non-zero parameter values detract from the negative impedance conversion properties of the NIC, and are termed parasitic immittances. It has been demonstrated by Larky [Ref. 14] and others that the parasitic parameters of some nonideal NIC's can be nulled out by compensation networks at the expense of an incremental change in

$h_{12}h_{21}$. These discussions though, have been restricted to the use of
NICs presenting only real immittances and are thus unsatisfactory for
high frequency NIC operation where complex immittances occur. In the
material below, consideration is given to overcoming the above failing.
Methods for providing compensation that do not effect the conversion
ratio are developed along with complex compensation networks.

Assume for the moment that a given NIC has the matrix parameters of
equation 22.

$$\begin{bmatrix} h_{11} \neq 0 & h_{12} \\ h_{21} & h_{22} \neq 0 \end{bmatrix} \tag{22}$$

Since the NIC is a non-reciprocal active device, in either the INIC or
VNIC modes, the cross product $h_{12}h_{21}$ is always greater than zero. The
determinant Δh, as well as h_{11} and h_{22} though, may assume either posi-
tive or negative immittance values. Probabilistically, it is possible
for a nonideal NIC to present any one of eight sets of h parameters at
a given frequency of operation. These are summarized in Table two.

set	h_{11}	h_{22}	Δh
1	≥ 0	≥ 0	< 0
2	≤ 0	≤ 0	> 0
3	≤ 0	≤ 0	< 0
4	≤ 0	≥ 0	< 0
5	≥ 0	≤ 0	< 0
6	≥ 0	≥ 0	> 0
7	≥ 0	≤ 0	> 0
8	≤ 0	≥ 0	> 0

Table 2

Set 7 and 8 are impossible combinations. For set 7:

$$h_{11} \geq 0, \ h_{22} \leq 0, \ \triangle h \geq 0, \ \text{given } h_{12}h_{21} > 0, \ \text{then}$$

$$h_{11}h_{22} \ (\leq 0) - h_{12}h_{21} \ (> 0) \not\geq \triangle h \geq 0 \qquad .$$

Likewise, for set 8:

$$h_{11} \leq 0, \ h_{22} \geq 0, \ \triangle h \geq 0, \ \text{given } h_{12}h_{21} > 0, \ \text{then}$$

$$h_{11}h_{22} \ (\leq 0) - h_{12}h_{21} \ (> 0) \not\geq \triangle h \geq 0 \qquad .$$

The remaining cases, 1 through 6, are possible resultant realizations that require compensation in order to assure proper NIC action. These cases are now considered in turn. As will become evident, it is fortunate that NIC's can in effect be considered self-compensating.

1. Set 1 $(h_{11} \geq 0, \ h_{22} \geq 0, \ \triangle h \leq 0)$

For the compensated NIC to have $h_{11_T} = 0$, h_{11} must be made zero. The subscript t is used to denote the matrix parameters associated with the overall compensated structure. Likewise, for $h_{22_T} = 0$, h_{22} must be made zero. Assume that an impedance S is placed in the output leg, while an impedance P is placed in shunt across the input of the network. The overall network is shown in Figure 30.
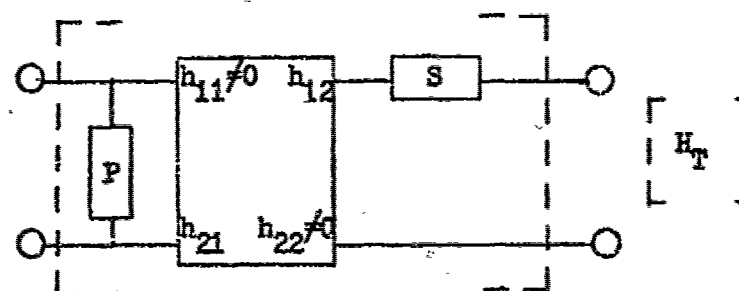

Fig. 30. Compensation Network for H Parameter Set 1

If the conversion ratio is indeed equal to one, then S is reflected to the input side as -Sx1, and P is reflected to the output

side as $-P/1$. Thus, choosing S and P properly results in h_{11} and h_{22} both going to zero value.

The overall H matrix for Figure 30 is equivalent to:

$$[H_T] = \begin{bmatrix} \dfrac{h_{11} + S\,\triangle h}{1 + h_{11}/P + h_{22}S + \dfrac{S}{P}\triangle h} & \dfrac{h_{12}}{1 + h_{11}/P + h_{22}S + \dfrac{S}{P}\triangle h} \\[4ex] \dfrac{h_{21}}{1 + h_{11}/P + h_{22}S + \dfrac{S}{P}\triangle h} & \dfrac{h_{22} + \triangle h/P}{1 + h_{11}/P + h_{22}S + \dfrac{S}{P}\triangle h} \end{bmatrix}$$

setting $h_{11_T} = 0$ and solving yields,

$$h_{11} + S\,\triangle h = 0 \Rightarrow S = -h_{11}/\triangle h \tag{23}$$

setting $h_{22_T} = 0$ and solving yields,

$$h_{22} + \triangle h/P = 0 \Rightarrow P = \triangle h/-h_{22} \tag{24}$$

Substituting the derived values of S and P into the $[H_T]$ matrix yields:

$$[H_T] = \begin{bmatrix} 0 & \dfrac{\triangle h}{-h_{21}} \\[3ex] \dfrac{\triangle h}{-h_{12}} & 0 \end{bmatrix} \tag{25}$$

In order to ensure a unity conversion factor, the new conversion factor $K' = \dfrac{\triangle h^2}{h_{21}h_{12}}$ must equate to one, where $h_{12}h_{21}$ equals the conversion factor of the uncompensated network. It can be seen from these relations that the reduction of the parasitic immittances has been achieved at the expense of reducing the original conversion ratio K to K' by a factor of $\dfrac{\triangle h^2}{(h_{21}h_{12})^2}$. This result implies that either the ratio K of the uncompensated network must be greater than one by a factor $(\dfrac{h_{12}h_{21}}{\triangle h})^2$, and hence the values S and P scaled accordingly, or $(\triangle h)^2 = 1$.

2. <u>Set 2</u> $(h_{11} \leq 0, h_{22} \leq 0, \triangle h > 0)$

This case is the direct dual of case 1; all signs of all pertinent parameters, $h_{12}h_{21}$ excepted, a reversed. Hence, the same compensation structure as used in Figure 30 may be utilized. The resultant H matrix yields identical S and P values as given in equations 23 and 24. Likewise, the reduction in K and the comments concerning the resultant ratio apply as they did in Set 1.

3. <u>Set 3</u> $(h_{11} \leq 0, h_{22} \leq 0, \triangle h < 0)$

The addition of an impedance S in series at the input and the shunting of P across the output should cause h_{11_T} and h_{22_T} to reduce to zero. This intuitive placement of compensation elements leads to the arrangement shown in Figure 31, where the H_T matrix is given by equation 26.

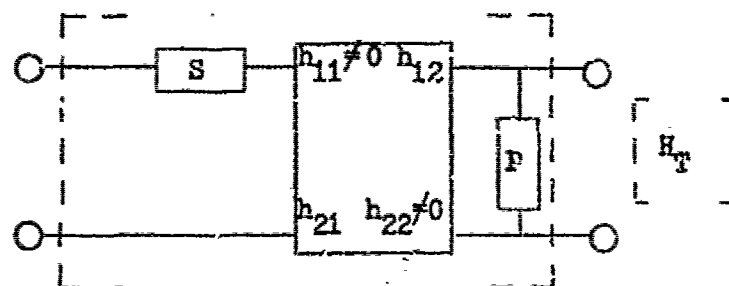Fig. 31. Compensation Network for H Parameter Set 3

$$[H_T] = \begin{bmatrix} h_{11} + S & h_{12} \\ h_{21} & h_{22} - \frac{1}{P} \end{bmatrix} \qquad (26)$$

Setting h_{11_T} and h_{22_T} equal to zero yields $S = -h_{11}$ and $P = -1/h_{22}$, respectively, with the H_T matrix reducing to the following:

$$[H_T] = \begin{bmatrix} 0 & h_{12} \\ h_{21} & 0 \end{bmatrix} \qquad (27)$$

38

It is to be noted that in this case there is no reduction in the conversion factor K; the placement of the impedances in the positions shown in Figure 31 results in $K^* = K$. In addition, this placement may be used with parameter values from set 2, with the added benefit of a constant K ratio.

4. Set 4, 5, and 6

Sets 4 and 5 are handled in the same manner as the previous sets covered. For each of these sets, though, there are two possible schemes for the placement of the elements S and P, one yielding a reduced K, the other a unity K. These are listed in Table 3.

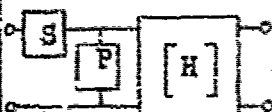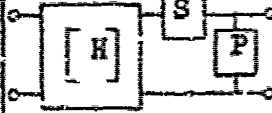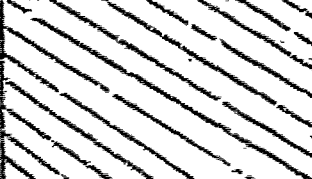The last set to be considered is set six ($h_{11} \geq 0$, $h_{22} \geq 0, \Delta h > 0$), which is of interest solely because there are no passive, positive real impedance values that lead to compensation. Consider the compensation scheme for set 1, where $S = \dfrac{-h_{11}}{\Delta h}$ and $P = \dfrac{h}{-h_{22}}$. Since Δh is specified to be positive, S and P would have to reduce to negative impedances. Consider the compensation scheme of set 3, where $S = -h_{11}$ and $P = -1/h_{22}$. Since h_{11} and h_{22} are now specified to be positive functions, S and P again reduce to negative impedances. If Δh is assumed to equal zero, then S and P must assume infinite values, while if $h_{11} = h_{22} = 0$, there is no need for compensation networks.

The conclusion then is that there is no passive, real positive function compensation scheme possible.

5. Summary

The following table summarizes the various compensation schemes considered above. The usefulness of these results rests in the fact that given any active structure that satisfies the listed h parameter specifications, a NIC results by the use of the indicated compensation method. Therefore, the problem of synthesizing the NIC reduces to that of synthesizing the S and P impedance networks, whether real or complex, required for compensation.

39

TABLE 3

SET	h_{11}	h_{22}	$h_{12}h_{21}$	h	COMP. STRUCTURE	Z VALUES	K' VALUE
1	≥ 0	≥ 0	> 0	< 0		$S = \dfrac{-h_{11}}{\Delta h}$	$\dfrac{\Delta h^2}{h_{12}h_{21}}$
2a	≤ 0	≤ 0	> 0	> 0		$P = \dfrac{-\Delta h}{h_{22}}$	
2b	≤ 0	≤ 0	> 0	≤ 0		$S = -h_{11}$	$h_{12}h_{21}$
3	≤ 0	≤ 0	> 0	≥ 0		$P = \dfrac{1}{-h_{22}}$	
4a	≤ 0	≥ 0	> 0	< 0		$S = \dfrac{h_{11}\Delta h}{h_{12}h_{21}}$ $P = \dfrac{-\Delta h}{h_{22}}$	$\dfrac{\Delta h^2}{h_{12}h_{21}}$
4b	≤ 0	≥ 0	> 0	≤ 0		$S = -h_{11}$ $P = \dfrac{h_{12}h_{21}}{h_{22}}$	$h_{12}h_{21}$
5a	≥ 0	≤ 0	> 0	≤ 0		$S = \dfrac{h_{11}}{h_{12}h_{21}}$ $P = \dfrac{1}{h_{22}}$	$h_{12}h_{21}$
5b	≥ 0	≤ 0	> 0	< 0		$S = \dfrac{-h_{11}}{\Delta h}$ $P = \dfrac{h_{12}h_{21}}{h_{12}\Delta h}$	$\dfrac{\Delta h^2}{h_{12}h_{21}}$
6	≥ 0	≥ 0	> 0	> 0	NONE		
7	≥ 0	≤ 0	> 0	> 0	NONE		
8	≤ 0	≥ 0	> 0	> 0	NONE		

H. NIC STABILITY CONSIDERATIONS

The ideal NIC, or its compensated nonideal equivalent, were modeled in Figure 16 and 17. Considerations of these representations leads one to the conclusion that at any frequency f_1 the NICs are absolutely stable. This is apparent since the illustrated models allow for no transient states.

Assume now that the ideal NIC is loaded as shown in Figure 32.
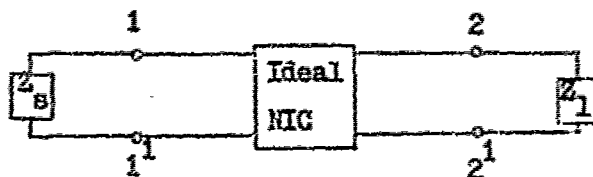
Fig. 32. Two Terminal Loaded Ideal NIC

If we consider Z_s and Z_1 to be passive impedances, the resultant system has a network determinant Δ given by $\Delta = (Z_s - Z_1)$. The roots of Δ, which are the natural frequencies of the overall system, are values of jw for which $Z_s = Z_1$. Since the natural frequencies are the zeros of the various circuit determinants, one approach would be to use the Routh-Hurwitz test to ascertain stability -- but only if the circuit determinant and the characteristic polynomial are easily obtainable.

Though the above approach is quite straight forward, it is often impractical to implement, since, in its basic form, a NIC is inherently a feedback amplifier. Thus stability is best determined by conventional feedback theory, and in particular, that due to Nyquist.

Consider again the NIC configuration of Figure 32. The impedance seen to the right of terminal pair 1-1' is $-Z_1$, that to the left, Z_s. The resultant mesh impedance is $Z_s - Z_1$, as pointed out above. If Z_1 should equal Z_s, then the total impedance would be zero, and any voltage

inserted in series with this mesh would call for an infinite current, an obviously impossible situation. Thus, it becomes evident that Z_1 should not equal Z_s, or equivalently, the ratio Z_1/Z_s should not equal $1/0$ if the system is to be stable.

The same general rule for stability can be arrived at by looking at the impedances as seen from the terminal pair 2-2'. The resultant impedance seen at 2-2' is $(Z_1 - Z_s)$. The term $-Z_s$ calls for a current flow 180° out of phase from that flowing through Z_s at port 1-1'. This implies that where the phase angle of Z_s equals that of Z_1, the magnitude of Z_s must be greater than that of Z_1. Phrased in an equivalent manner, if the phase angle of Z_s equals the phase angle of Z_1, the magnitude of Z_1/Z_s must be less than unity. Thus, the ideal NIC will be unconditionally stable provided that the magnitude of Z_1/Z_s is less than unity at any frequency where the angle of this ratio is zero.

If we allow $Z_s \neq Z_1$, then it should make no difference if we interchange the positions of Z_s and Z_1. The conclusion to be drawn is that if the overall circuit of an ideal NIC plus terminations is stable, so also is the system obtained by transposing the terminating load impedances. In practice, actual NICs do not, in general, behave in this manner. It is observed that when unequal impedance terminations are interchanged, the system goes from stable to unstable.

This can be explained by recalling the fact that a NIC must employ positive feedback to achieve the required H matrix, and that under certain terminating conditions, the system may satisfy the requirements to permit operation as a phase shift oscillator.

It has been shown by Brownlie [Ref. 15], that a two port network that functions as a NIC at low frequencies inevitably has an unstable

42

mode of operation when one terminal pair of the device is open-circuited, and the other terminal pair short-circuited. Though Brownlie's approach is intrinsically more attractive, since it involves a fundamental limitation on the behaviour of the active device, a more direct approach may be given.

Assume an ideal NIC with the matrix of equation 11. However closely the measured h parameters of the actual device may approach the conditions expressed by this assumption, they must, in reality, depart from the ideal case in an appropriate manner [Ref. 16].

Consider some amount of time delay T for transmission across the device, where $f(t) \rightarrow f(t-T)$, then in the frequency domain $f(p) \rightarrow e^{-pt}F(p)$. Consider the NIC to be redefined by the relations

$$h_{11} = h_{22} = 0 ,$$

$$h_{12}h_{21} = e^{-pt} . \tag{28}$$

If T is exceedingly small, the NIC will closely approximate the behaviour of the ideal representation. Assume terminating impedances Z_s and Z_1, placed as shown in Figure 32. Then, the zeros of Δ_h are those values of $p = \sigma + jw$ for which:

$$\frac{Z_s}{Z_1} = e^{-\sigma t} (\cos wt - j\sin wt). \tag{29}$$

When this ratio of terminating impedances is positive real, is given by $w = 2\pi n/t$, $n = 0, \pm 1, \pm 2...$. Solving for p by taking the logarithm of both sides of equation 29, it is clear that if $Z_s > Z_1$, the logarithm is real and negative, and the zeros of $+ jw$ are all in the left hand plane; if $Z_1 > Z_s$, the logarithm is real and positive, and all the zeros are in the right hand plane. Hence, if a NIC is defined by equation 28 and is terminated at ports 1-1' and 2-2' with impedances Z_s and Z_1

43

respectively, the resulting system is stable or unstable according to whether Z_s is greater or less than Z_1.

I. ANTENNA MATCHING USING NIC's

Having considered the realizability of the negative capacitance element, our attention is now redirected to the initially posed antenna matching problem.

1. Matching By Conjugate Immittance Synthesis

If the forms of the antenna impedance $Z(s)$ is prior knowledge, it is possible to synthesize from it the equivalent antenna $X(s)$ function and represent it in terms of lumped, realizable elements.

The function $X(s)$ which we wish to synthesize has its representation as a quotient of polynomials of real coefficients and has been extensively studied and reported on, especially with regard to active RC filter applications. The primary RC driving point synthesis procedure of importance is due Kinariwala [Ref. 17]. Though our concern is directly with RC representable antenna forms, it is worthy of note that synthesis procedures also exist for the RL (Sipress) [Ref. 18] and RLC (Rohrer) [Ref. 19] lumped element networks. All of the above methods and procedural forms are well documented and hence will not be reviewed here. For specific details, the reader is referred to the cited references.

Assume that the antenna impedance characteristics are known. Then, the procedure is to extract the reactive portion of the impedance and represent it in polynomial form. Then, one of the above driving point synthesis procedures is employed to reduce the reactive characteristic to a realizable lumped element configuration. In its simplest form this reduces to, for instance, saying that a short top-loaded antenna is representable by a resistance R and capacitor C_1, and hence, the synthesis

of the reactive antenna component is a capacitor of value C_i. For
general purposes, though, we represent the synthesized network as an
RC, RL, or RLC network, as shown in Figure 33b.
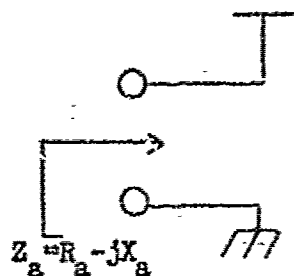
Fig. 33a. Antenna Impedance
           Assumed
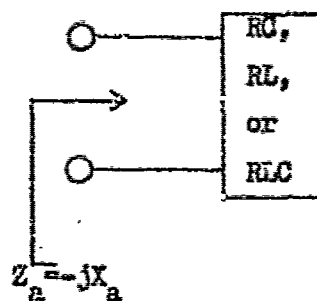
Fig. 33b. Impedance Characteristics
           of Discrete Network
           Assumed

If this synthesized value of the imaginary portion of the antenna
impedance is now placed as the load of a converter circuit, we are able
to realize the negative of the reactive portion of the antenna as depicted
below.

Fig. 34. Means of Realizing Conjugate
          of Antenna Impedance

In series form, the antenna matching network would be configured
as in Figure 35a, in parallel form, as in Figure 35b.
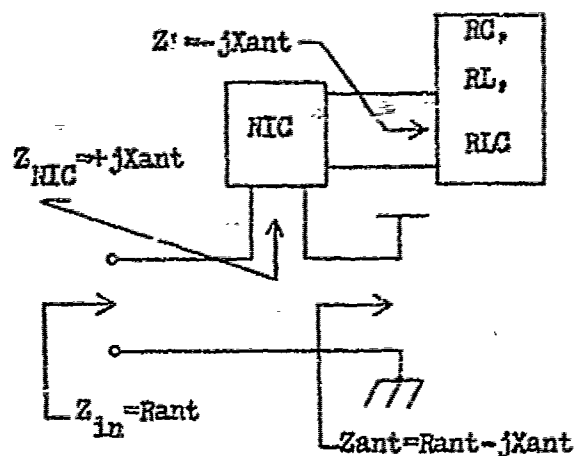
Fig. 35a. Series Antenna Matching Network
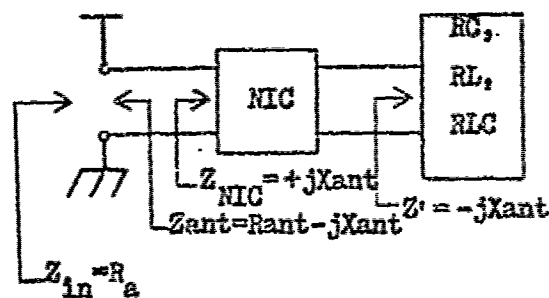
Fig. 35b. Parallel Antenna Matching Network

2. Conjugate Stub Matching

For a fixed site, environment independent location the above con-jugate immittance synthesis matching procedure is practical, although the assumed conditions may not be. The inherent p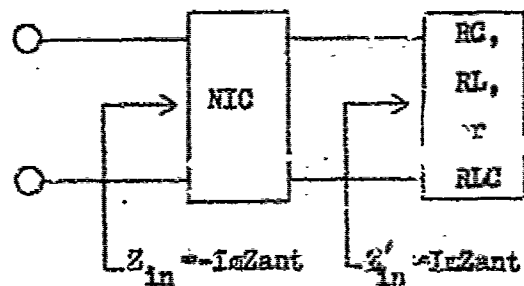roblem is, of course, that the antenna parameters are variable, hence the synthesized network would have to vary accordingly in order to assure a resonance match, especially at higher frequencies, where the structure capacitance itself is variable and independent of surroundings.

This problem can be effectively eliminated if the synthesized antenna network is replaced by a second antenna with terminal character-istics essentially identical to the antenna utilized in the above procedure.

46

It is again assumed that the antennaes utilized are electrically short, highly capacitive top loaded probes. Hence, the summation of the antenna resistance factors results in an extremely small total resistive component, and the impedance converter is effectively reflecting only a lumped capacitive reactance; i.e., the imaginary portion of the antenna impedance. In fact, the resistive component of such small antennaes is approximately two orders of magnitude less than the reactive portion up to a frequency of roughly hundreds of Megahertz. Nevertheless, if reflected negative resistance presents any major problem, it can be eliminated by placement of series or shunt resistances.

Placing the second antenna as the load of an ideal NIC, leads to the series matching scheme of Figure 36a and the parallel configuration of Figure 36b.
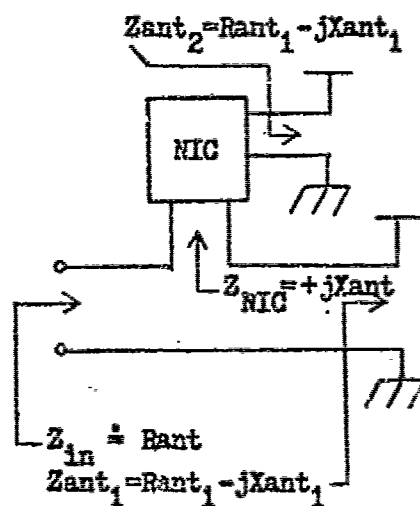

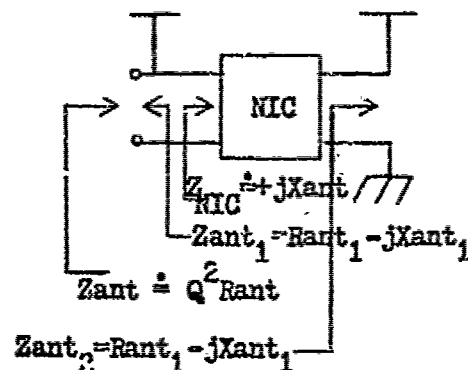Fig. 36a. Series Conjugate Antenna
           Matching Scheme

Fig. 36b. Parallel Conjugate
           Antenna Matching Scheme

47

III. EXPERIMENTAL PROCEDURES

Experimental methods used were broken into two catagories; those related to the testing of individual converter circuits, and those related to the testing of the overall miniature antenna system. In each case, conventional testing methods proved unsatisfactory and had to be modified as discussed below.

A. CONVERTER CIRCUITS

Two distinctly different parameter measurement schemes had to be developed for testing the various type of converter circuits. The first method applied to the testing of the ideal generator model realization, the second to the matrix models constructed.

1. Ideal Generator Testing Procedures

This class of converter was tested in a relatively simple, straight forward method. For the circuit configuration of Figure 21, it was only necessary to assure that the output voltage was equal to $2 \cdot V_{in}$ over the frequency range of interest. Because high input, low output resistance operational amplifiers were used in the actual circuits, the input-output impedance requirements were approximately satisfied.

2. Matrix Model Testing Procedure

NIC circuits based on a matrix realization have been shown to have one open-circuit stable (OCS) port, and one short-circuit stable (SCS) port. As a result of this phenomenon, it is characteristic for an NIC to be stable if the impedance loading of the OCS port is large and that of the SCS port is small. Since it was impossible to accommodate the loading requirements of the two different orientations within

one test setup, it was necessary to employ several different measurement schemes in order to measure the parameters of interest.

For a first order approximation, the individual circuits were modeled and run on a computer using the Electronic Circuit Analysis Program [Ref. 21]. Though this method was only as accurate as the active device representations, it did allow for the determination of an accurate low frequency H matrix. Based on these results, the converters were compensated to within an order of the correct magnitude, and then the net result reprogrammed for a second run to assure that the intended effect was obtained.

The next procedural step was to assure that the NIC possessed a unity conversion ratio. The conversion ratio $h_{12}h_{21}$ of the NIC was measured by means of the test arrangement shown in Figure 37.
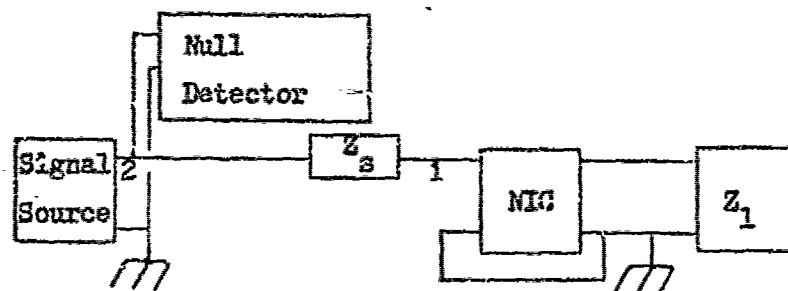
Fig. 37. Test Setup for Measuring the NIC Conversion Ratio

For this figure, the impedance to the right of point 1 is given by:

$$Z_1 = h_{11} - \frac{h_{12}h_{21}Z_1}{1 + h_{22}Z_1},$$

while that to the right of point 2 is:

$$Z_2 = Z_s + h_{11} - \frac{h_{12}h_{21}Z_1}{1 + h_{22}Z_1}. \qquad (30)$$

Since all converter circuits used in this test configuration had $h_{11} \doteq h_{22} \doteq 0$, equation 30 reduces to $Z_2 \doteq Z_s - h_{12}h_{21}Z_1$. For the initial K

adjustment, Z_s was set equal to Z_1 and the NIC circuit values were varied until a voltage null appeared at point 2. When such a null occurred,

$$\frac{Z_s}{Z_1} = h_{12}h_{21} = K \text{ circuit under test}$$

and the actual conversion ratio was thus observable.

Figure 38 shows the measurement setup used to duplicate the block diagram arrangement of Figure 37. A GR 1606 RF Impedance Bridge, which presents a sufficiently high impedance to the load to prevent oscillation, was used for the impedance Z_s. The oscilloscope was employed to monitor for signal distortion and possible circuit oscillations, but was removed during the actual measurement tests.
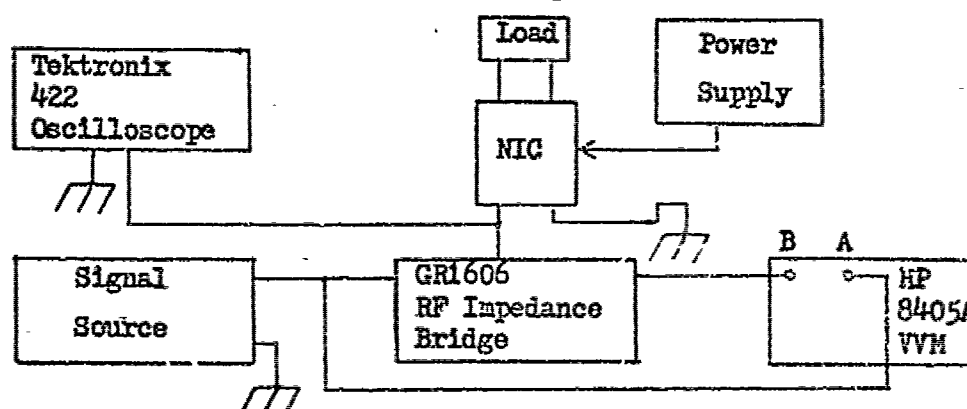

Fig. 38. Voltmeter Null Detector Arrangement for Measurement of $h_{12}h_{21} = K$

In order to measure the actual input impedance presented by the loaded converter circuit, a low impedance (50 ohms) measurement arrangement using a H.P. Vector Voltmeter was utilized in the configuration of Figure 39,
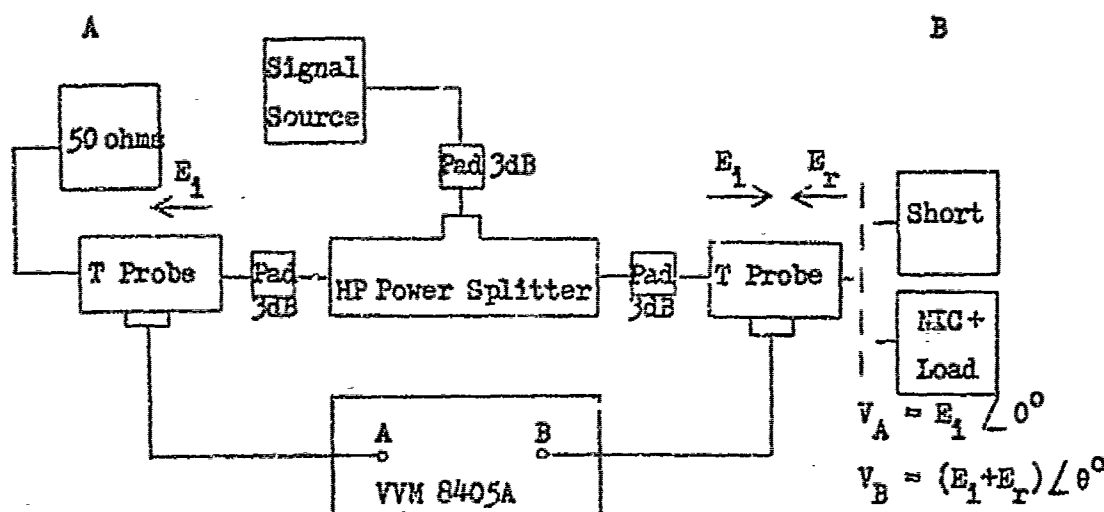
Fig. 39. Vector Voltmeter Test Circuit for Measuring Converter
Input Impedance

The Vector Voltmeter compares the incident voltage, E_i, at the 50 ohms
load with the voltage $E_i + E_r$ at the NIC; the quantity actually measured
is thus $1 +$, which was easily converted to values of Z by use of Smith
Charts. The system was first calibrated using a short circuit load in
order to compensate for differing line lengths and other sources of un-
desired phase shift.

Knowing the conversion ratio and the converted input impedance
for a given load, it was then possible to optimize the converter by trial
and error so as to insure the desired performance characteristics.

B. ANTENNA SYSTEM TESTING

The basic means of testing the various active broadband conjugate
antenna systems was to compare its performance against a reference re-
ceiving antenna, in this case a 12 foot, untuned Tricor whip. The basic
antenna structure used with the active networks was a two inch in length,
$\frac{1}{4}$ inch in width rod that had a one inch in diameter by one inch in length
cylindrical, solid, rod mounted atop.

To compare their respective performance, the configuration of Figure 40 was employed.
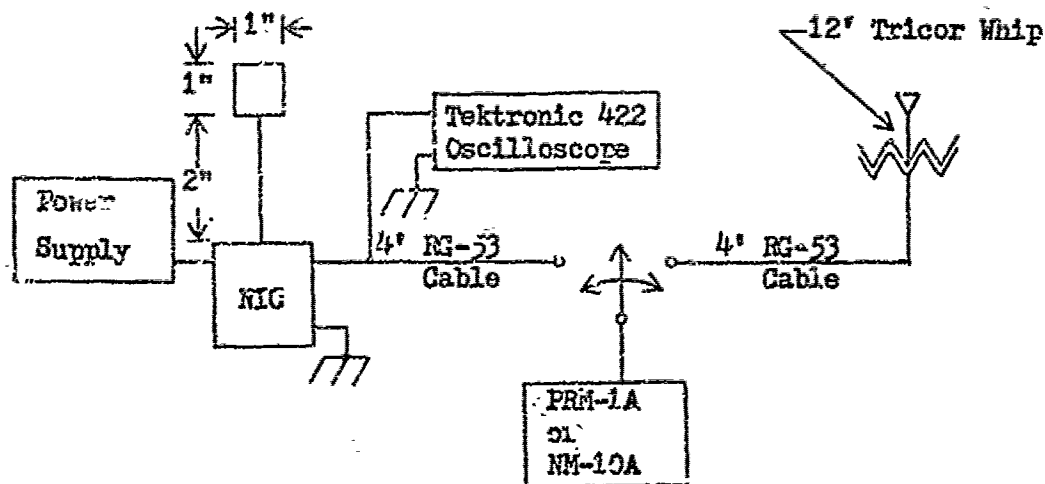
Fig. 40. Method Used for Obtaining Comparison Reception Data

Depending on the frequency of interest, either a PRM-1A, or a NM-10A, Radio Test Set was used to obtain comparison signal level measurements from each of the two antenna systems. The active network contained in Figure 40 was constructed from the theory of chapter three and had either the synthesized passive element feedback network, or a second matching antenna included as an integrated element. The Tektronix 422 Oscilloscope was used to monitor for active network instabilities and was removed during actual testing. Lastly, all tests on the antenna systems were conducted at the antenna roof facilities of the Naval Postgraduate School.

IV. RESULTS

Based on the theory presented in chapter two, three basic active antenna systems were designed and tested. In the sections below, the design requirements and means of satisfying them are discussed. Then, the method by which each was used to obtain a conjugate matched antenna system is presented along with the test data obtained.

A. IDEALIZED GENERATOR VNIC MODEL

Based on the theory developed in chapter two, an idealized generator VNIC model was constructed. The resultant product was tested using both a simulated, discrete element, antenna impedance, and with an antenna placed in the feedback loop.

Section one discusses the simulated antenna model, section two the antenna feedback derivation, while section three provides an analysis of the systems with respect to the data obtained.

1. Idealized Generator VNIC Model with Discrete Component Feedback Network

The circuit shown in Figure 21 was constructed using commercially available wideband differential FET input operational amplifiers. The pertinent characteristics of the selected operational amplifiers, Burr-Brown 3400 A's, are given in Table 4, while the actual circuit form employed to implement Figure 21 is shown in Figure 41.

Consideration of Figure 41, with Z_i removed, showed that the input impedance of the overall network is approximately the input impedance of the first operational amplifier stage, while the output impedance is less than an ohm for frequencies under 20 MHz.

TABLE 4

Burr-Brown 3400A Operational Amplifier Characteristics

Rated output	$\pm 10V$
Unity gain BW	100 MHz
Open loop gain	90 dB
Open loop input Z_i	10^n ohms, 2pF
Open loop output Z	25 ohms at 10 MHz

Fig. 41. Idealized Generator VNIC Circuit
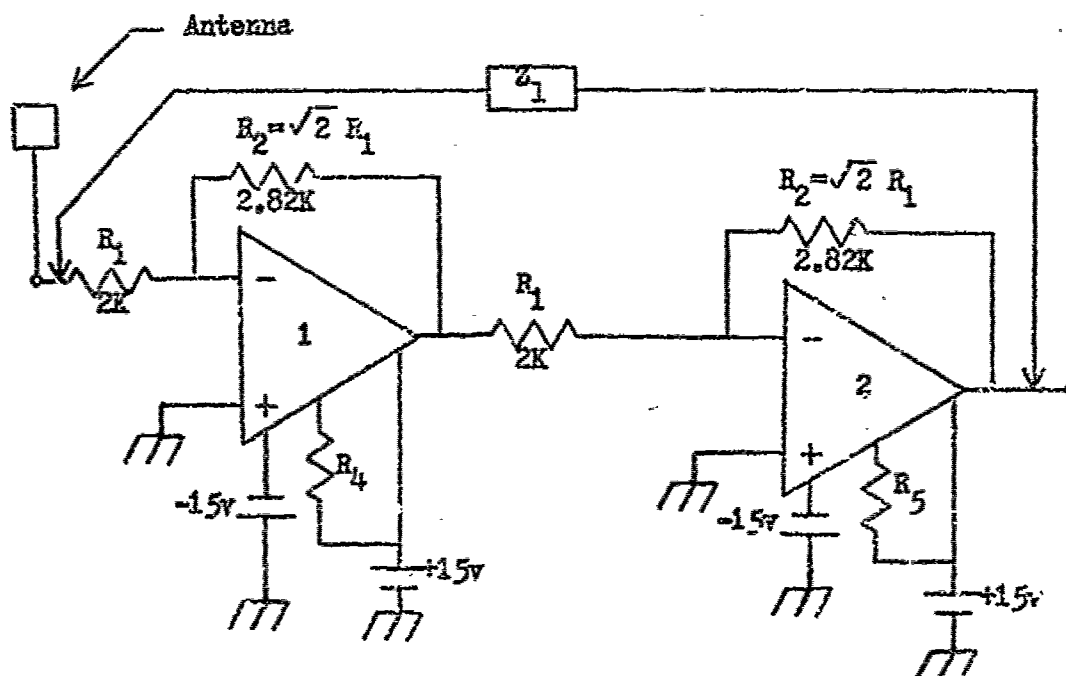
Resistances R_2 and R_3 were adjusted to give a total gain of two at the output terminals. It was found that this gain could be maintained up to 43 MHz without the need of circuit modifications. R_4 and R_5 are 261 ohms resistors used for DC nulling.[3]

---

[3]All power supplies shunted to ground by the parallel placement of .02 uf ceramic and 10 uf tantalum capacitors.

It was assumed that the antenna was indeed capacitive in nature, and hence a feedback network, Z_1, composed of a parallel placed variable capacitor, 10-100 pF, and a resistance 0-1 K, were used to simulate the conjugate of the antenna impedance. The resistance was inserted to provide a means of fine tuning the reflected negative impedance. The final form of the network, with Z_1 in place, equated to the parallel antenna matching network of Figure 35b.

For purposes of testing, a PRM-1A was used in the test setup of Figure 40. A frequency was selected where a signal was present, and then the respective signal strength from each antenna system was recorded. The results are presented in Figure 42, where gain vs frequency of the active conjugate matched antenna relative to that of the untuned 12 foot whip is shown. Though this figure serves to show the merit of the concept, the results were actually severely degraded for three basic reasons.

First, since the operational amplifiers were restricted to an output swing of $\pm$ 10 volts, care had to be exercised if circuit damage was to be avoided. Because of the presence of a neighboring 1 kilowatt transmitter site (KMBY, 1240 KHz), approximately three miles distant, and the fact that the antenna system responds to all incident signals, the circuit feedback network had to be tuned so that the operational amplifier output restrictions were met. It was noted that if the feedback capacitance was increased over 21 pF, the output signal from KMBY rapidly reached a point in excess of the $\pm$ 10 volts output limitation. It is worthy of note that this fact was learned at the expense of one operational amplifier that could not sustain a near resonance output swing of $\pm$ 33 volts, as monitored on a Tektronix 422 oscilloscope.
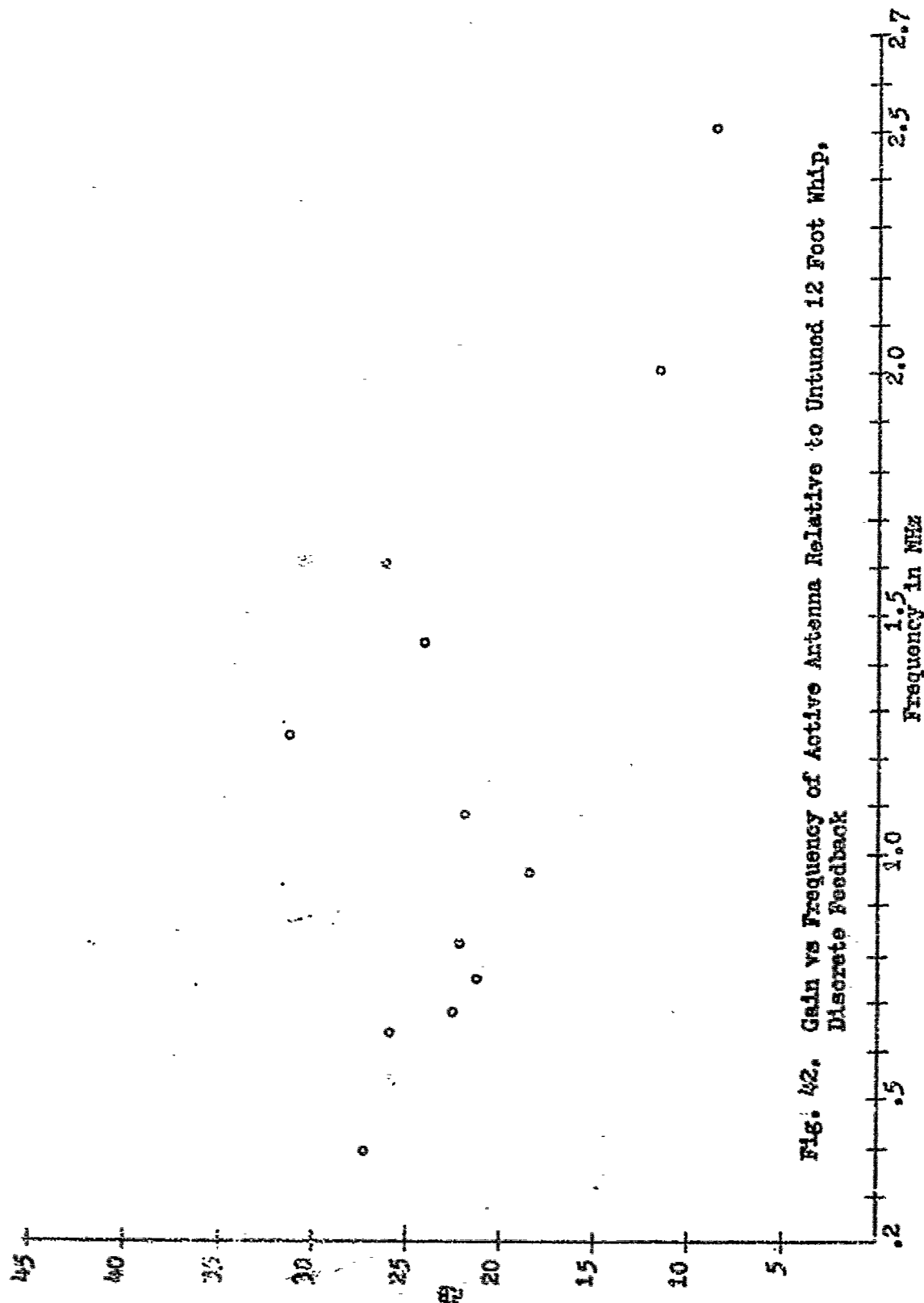
Fig. 42. Gain vs Frequency of Active Antenna Relative to Untuned 12 Foot Whip, Discrete Feedback

59

Secondly, even if the output signal level was maintained under the $\pm$ 10 limit, it was evident that the RF and IF sections of the receiver test sets used would be incapable of handling such high signal levels without being completely saturated. For the PRM-1A employed during testing, the maximum input level that did not cause saturation was approximately .6 volts at the input terminals. Hence, the maximum input signal at any frequency incident and responding through the active antenna network had to be limited to .6 volts.

Lastly, the amount of "detuning" permissable, achieved by variance of either the capacitor or resistor within the feedback network, was limited to values that resulted in stable system operation.

As a means of determing the relative performance of the active system, the test setup was removed to a signal isolated environment, and exposed to individually radiated constant level signals. Such test signals were obtained by using a signal generator with its output terminated at the center of a four inch by four inch aluminum plate. The active antenna system was placed approximately two feet from this source and the signal strength received was measured with either the PRM-1A or the NM-10A. The results are shown in Figure 43, where gain over the untuned miniature antenna is plotted vs frequency. It was observed that as the values of elements used in the feedback network were varied, the curve tended to shift to the right or left, but always fell off to unity gain above the untuned antenna at approximately 43 MHz. Examples of these curves for various feedback network values are plotted in Figure 44. The unity gain value of 43 MHz compares favorably with results based on considerations of the anticipated unity-gain bandwidth product for the operational amplifiers used.
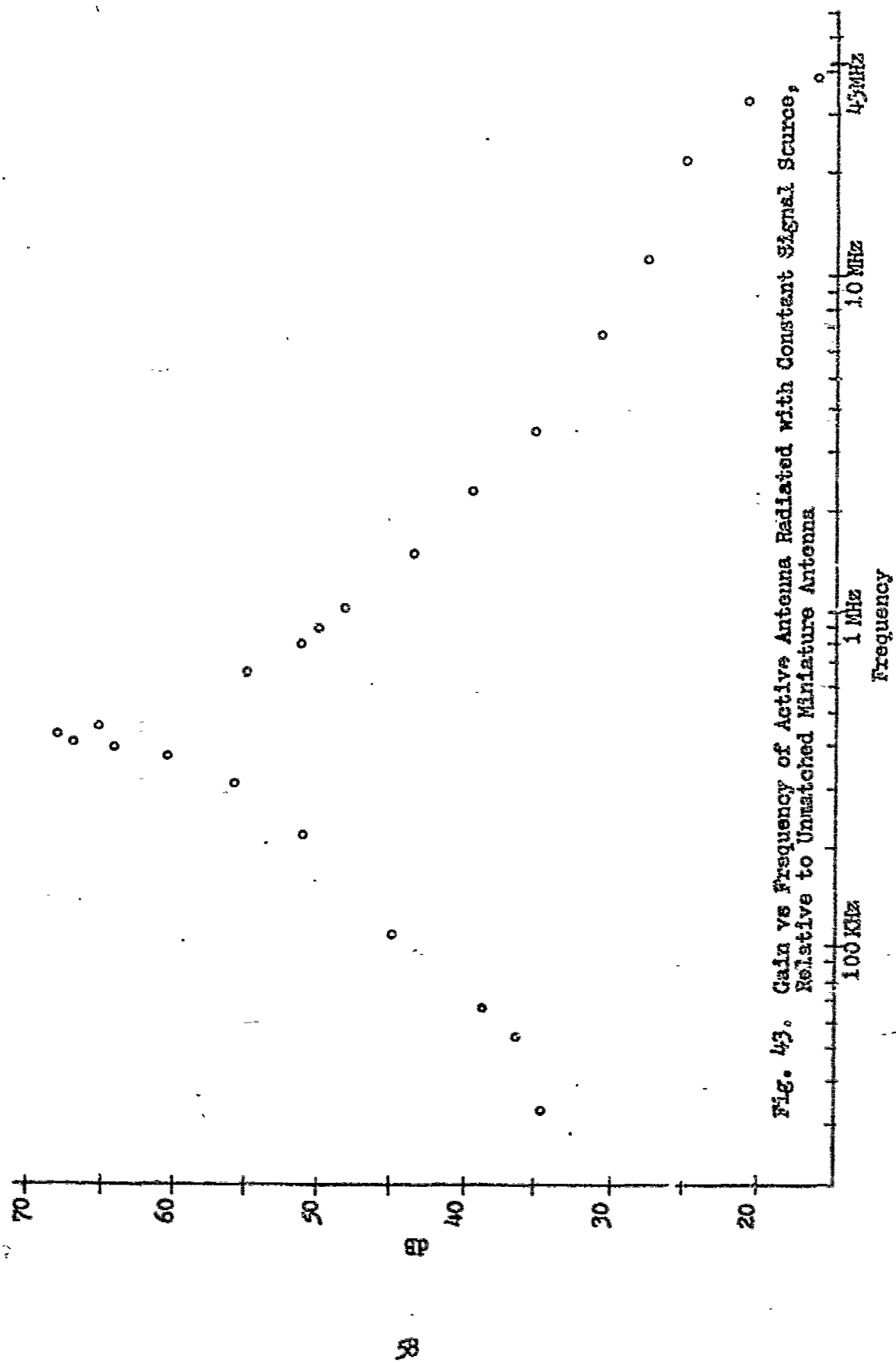
Fig. 43. Gain vs Frequency of Active Antenna Radiated with Constant Signal Source, Relative to Unmatched Miniature Antenna
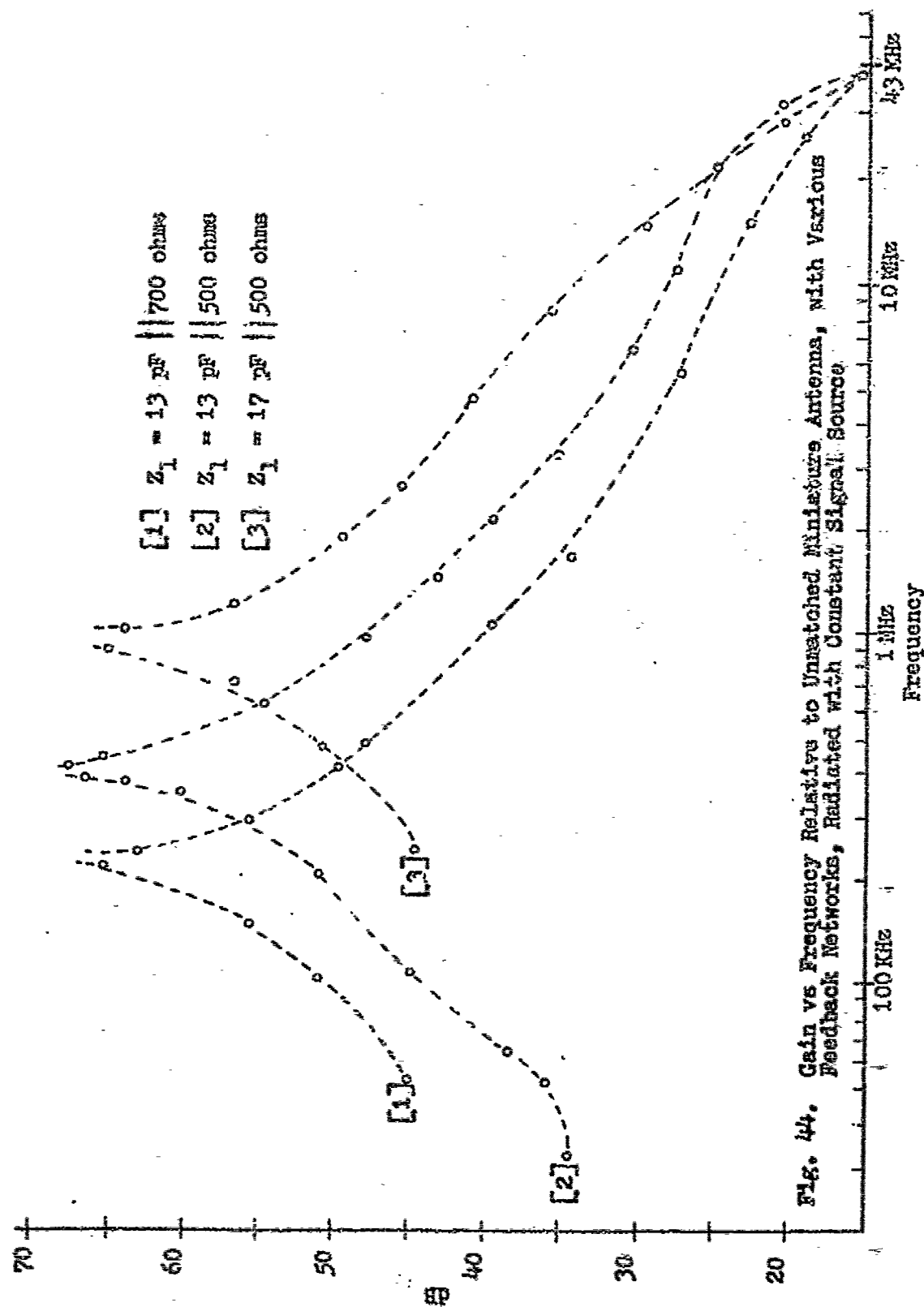
58

Fig. 44. Gain vs Frequency Relative to Unmatched Miniature Antenna, with Various Feedback Networks, Radiated with Constant Signal Source.

[1] $Z_1 = 13$ pF $||700$ ohms
[2] $Z_1 = 13$ pF $||500$ ohms
[3] $Z_1 = 17$ pF $||500$ ohms

2. Idealized Generator VNIC Model With Antenna Inserted In The Feedback Network

The configuration of Figure 41 was retained, but for this part the feedback loop was modified to that shown in Figure 45, thus leading to the equivalent of the two antenna systems shown in Figure 36b.
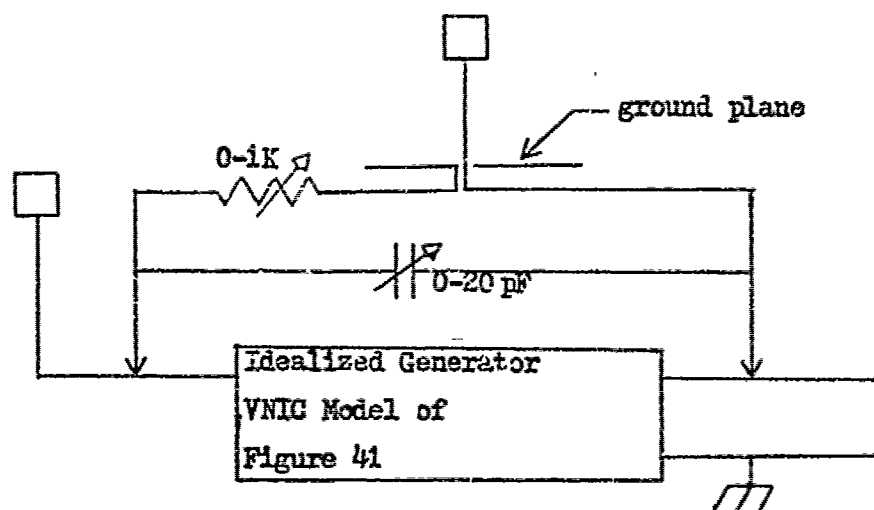

Fig. 45. Modified Feedback Arrangement Used to Approximate the Configuration of Figure 36b

With the feedback loop inserted, the active antenna system was tested following the same procedure employed in testing the discrete element feedback model. The previously noted restrictions concerning output voltage swings and stability considerations likewise applied to this circuit form. The results obtained are given in Figure 46, where once again gain vs frequency of the active conjugate matched antenna relative to that of the untuned 12 foot whip is plotted. With one exception, Figure 46 is the duplicate of Figure 42, but shifted up approximately 9 dB. This was attributed to a closer resonant matching, achieved without violating the stability restrictions for operation.

As with the first model, a controlled signal environment test was run, the results of which were for all purposes, identical to those shown in Figures 43 and 44.

60

Fig. 46. Gain vs Frequency of Active Antenna Relative to Untuned 12 foot Whip, Antenna Inserted in Feedback Loop
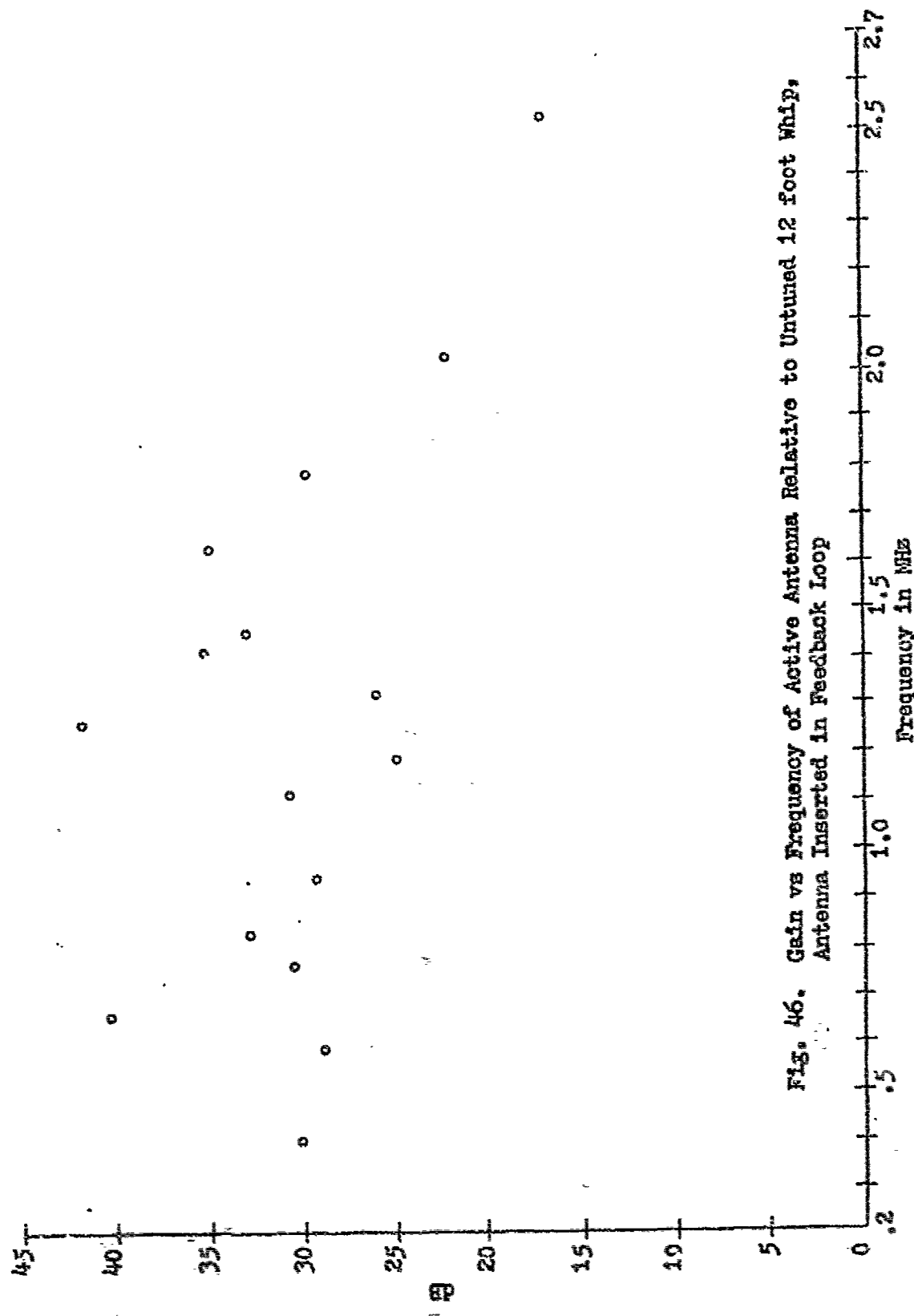
3. Analysis

The concern of this section is directed at considering the frequency response of the circuit utilized. The limitations previously discussed with respect to resonance 'detuning' due to output signal level restrictions and receiver input characteristics, are limitations apart from the conceptual problem of interest.

For the moment, assume that the above idealized generator model has an output impedance equal to zero, and a fixed, frequency independent, voltage gain equal to two. For frequencies less than 43 MHz, these approximations are empirically correct.

The resultant network is then modeled as shown in Figure 47, where Z_{in} represents the input impedance of the network, and Z_1, the inserted impedance of the feedback loop.
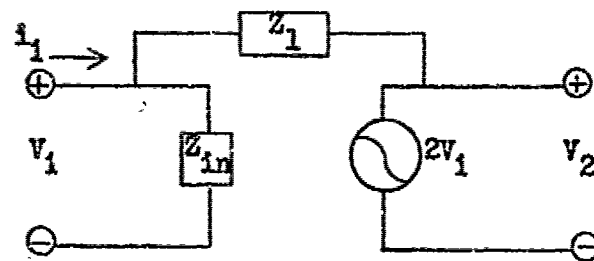
Fig. 47. Idealized Model of VNIC Generator

The input impedance for the overall circuit is equal to

$$Z_{in \; circuit} = -Z_1 \left[\frac{1}{1 - Z_1/Z_{in}} \right]. \qquad (31)$$

From the circuit form of Figure 41, and the characteristics of the operation amplifiers used, Z_{in} equates to

$$Z_{in} = -Z_I + \frac{Z_f Z_I}{Z_f + Z_1 \; (1+A_f)} \qquad (32)$$

where $Z_I = R_1$, $Z_f = R_2$, as shown in Figure 41, and A_f and Z_1 are as specified in Table 4. Substituting equation 31 into equation 32, yields

$$Z_{\text{in circuit}} = -Z_1 \left[\cfrac{1}{1 - \cfrac{Z_1(Z_f + Z_1(1+A_f))}{2Z_f Z_I + Z_I(Z_1(1+A_f))}} \right] \quad (33)$$

In equation 33, $Z_f \ll Z_1(1 + A_f)$ and $2Z_f Z_I \ll Z_I Z_1(1 + A_f)$ for frequencies less than 20 MHz. Thus equation 33 reduces to:

$$Z_{\text{in circuit}} = -Z_1 \left[\frac{1}{1 - Z_1/Z_I} \right] \quad (34)$$

If Z_1, the impedance of the feedback network, was composed solely of a capacitance, then $Z_{\text{in circuit}}$ would equate to

$$Z_{\text{in circuit}} \doteq \frac{1}{Z_I - jwC} \doteq \frac{-1}{jwC} \text{ for } Z_I \gg \frac{1}{wC}$$

and a severe low frequency restriction would arise.

To alleviate this problem, let Z_1 be a parallel capacitor, resistor network as employed in the actual models. Under these conditions, $Z_1 \approx \frac{R}{RCs+1}$, and $Z_{\text{in circuit}}$ reduces to

$$Z_{\text{in circuit}} = \frac{-R}{RCs + 1} \left[\cfrac{1}{1 - \cfrac{\frac{R}{RCs+1}}{Z_I}} \right]$$

$$Z_{\text{in circuit}} = \frac{-R}{RCs + 1 - \frac{R}{Z_I}}$$

$$Z_{\text{in circuit}} = \frac{-1}{jwC + \frac{1}{R} - \frac{1}{Z_I}} \doteq \frac{-1}{jwC} \text{ for } wC \gg \frac{1}{R} - \frac{1}{Z_I}$$

The result is twofold. First, a degree of control, within the limitations of the stability restrictions, is obtained using the variable resistor as an impedance adjusting element. Secondly, the rigid low

frequency restriction, $Z_I \gg \frac{1}{wC}$, previously mentioned, is traded off for a more reasonable high frequency limitation, $wC \gg \frac{1}{R} - \frac{1}{Z_I}$. This is especially advantageous, considering the low valve of C employed, typically less than 15 pF.

The effect of a finite output impedance is equally detrimental, but to a much lesser degree. This is primarily because the output of the last stage is approximately

$$Z_{out\ circuit} \doteq Z_{out\ 2nd\ AMP} \left[\frac{1}{1 + (Z_I/Z_f)\ A_f} \right] ,$$

and upon substitution of the actual circuit parameter values, $Z_{out\ circuit}$ reduces to less than 2 ohms up to 25 MHz, approximately a short circuit for analytical purposes. Hence, the input, output characteristics of the overall network are satisfied.

B. DISCRETE NONIDEAL NIC MODEL

Based on the derived theory for construction of nonideal NIC networks, an INIC model was constructed. The final antenna system, the result of several computer and actual testing iterations, was tested in the same manner as the idealized generator VNIC model.

1. Design Procedure

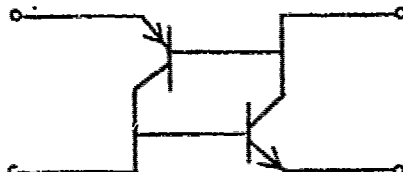The basic transistor configuration selected for modeling is shown without biasing elements in Figure 48.

Fig. 48. Transistor Arrangement Used in Modelling
the Nonideal NIC

64

The active device selected for use was a MD 6002, npn-pnp, single unit pair. In the circuit form of Figure 48, the H parameters are $h_{11} > 0$, $h_{22} > 0$, and $\Delta h < 0$, which satisfies the requirements imposed by Table 1.

In actuality, the form of Figure 48 is quite old, due initially to Yanagisawa [Ref. 20] and has been modeled in transistor form by several authors [Ref. 22 and 23].

If one considers the idealized version of the above circuit, as shown in Figure 49, it is evident that

$$V_1 = V_2$$

and

$$\frac{I_1}{I_2} = \frac{MR_2}{(M + 1) R_3 + R_2} \quad .$$
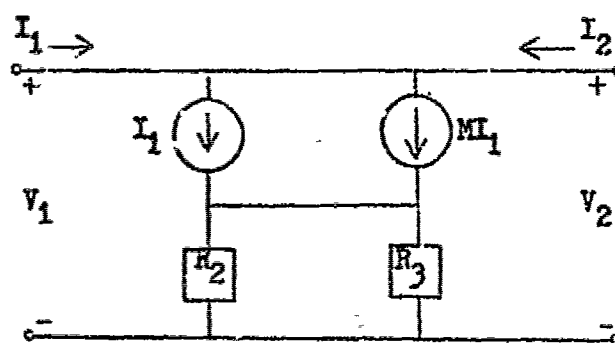
Fig. 49. Idealized Version of Transistor form Employed

Thus, for a large current generator factor M,

$$\frac{I_1}{I_2} \doteq \frac{R_2}{R_3}$$

where, with $R_2 = R_3$, I_1 closely approximates I_2 and the H matrix reduces to that of an ideal INIC.

In practice, each transistor must have a collector supply resistance, however, if these are identical and the NIC conversion factor is -1, then the collector resistances cancel one another. The addition of

these biasing elements result in the circuit form shown in Figure 50,
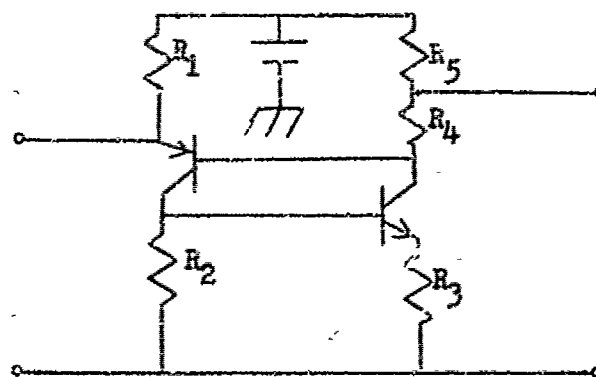
Fig. 50.   Biased NIC Configuration

and the small-signal equivalent circuit given by Figure 51.
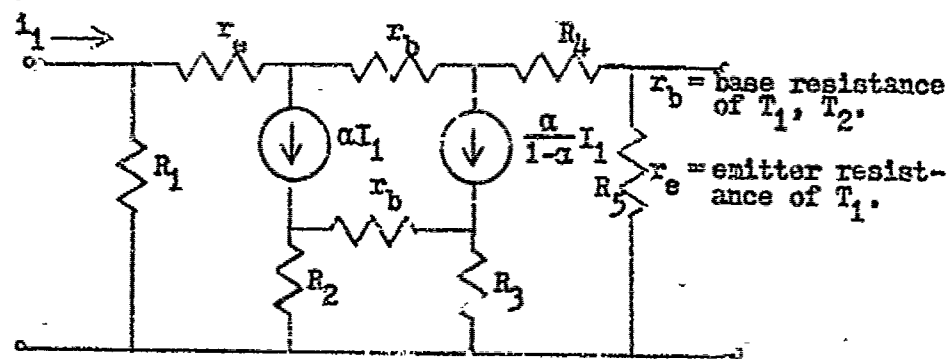
Fig. 51.   Small-Signal Equivalent of Figure 50

In order to insure that the collector resistances do cancel and that a transmission ratio of -1 is obtained, it was necessary to solve for the values of the various resistances in terms of each other. This was most easily done by using the Transmission Parameters, where

$$V_1 = AV_2 - BI_2$$

$$I_1 = CV_2 - DI_2$$

By requirement,

$$[H] = \begin{bmatrix} 0 & 1 \\ 1 & 0 \end{bmatrix} \Rightarrow [T] = \begin{bmatrix} 1 & 0 \\ 0 & -1 \end{bmatrix}$$

thus, $\dfrac{V_1}{V_2} = A\Big|_{I_2=0} = 1$, and $\dfrac{I_1}{V_2} = C\Big|_{I_2=0} = 0$

66

from which the following were obtained:

$$(2\alpha - 1) R_5 = R_1 \qquad (34)$$

$$R_2 = \frac{(2\alpha - 1)\left[R_3 + R_e + (1-\alpha)r_b\right]}{4\alpha^2 - 4\alpha + 1}. \qquad (35)$$

Using $\dfrac{V_1}{I_2} = -B\Big|_{I_2=0} = 0$, and $\dfrac{I_1}{I_2} = -D\Big|_{I_2=0} = -1$

yielded the last relationship, $(2\alpha - 1)R_4 = r_e + r_b(1-\alpha)$. $\qquad (36)$

If it is assumed that α is real, and equal to 1, then equations 34 through 36 reduce to:

$$R_5 = R_1$$

$$R_2 = R_3 + r_e$$

$$R_4 = r_e$$

Though the above procedure results in convenient circuit inter-relationships, it does not allow for the true AC operation since transistor capacitances were omitted. Still, it serves as a starting point for the required iterative processes necessary to achieve the final design.

Modeling the active device by the hybrid pi layout of Figure 52, Figure 53 was run using ECAP in order to determine the frequency vs H parameter characteristics of the network.
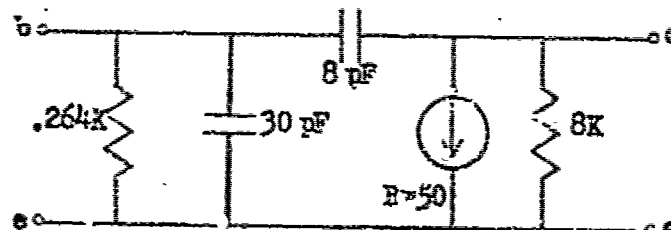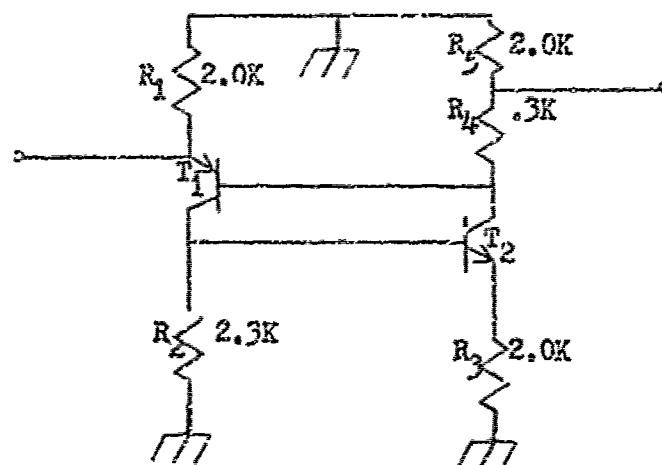

Fig. 52. Hybrid Pi Representation of Active Devices

Fig. 53. Circuit Form Run Using ECAP

An extract of the results obtained is given in Table five.

TABLE 5

f	h_{11}	h_{12}	h_{21}	h_{22}
1KHz	$39.68 \angle 180^\circ$	$1.016 \angle 0^\circ$	$.897 \angle 0^\circ$	$.794 \cdot 10^{-5} \angle 90^\circ$
1MHz	$40.98 \angle 147.85^\circ$	$1.014 \angle 0^\circ$	$.899 \angle 0^\circ$	$.792 \cdot 10^{-5} \angle 87^\circ$

For the cross product of $h_{12}h_{21}$ to equal 1, it was next necessary to increase the parameter h_{21} by modifying the value of R_4. By an iterative computational process, the value of $R_4 = 2260$ (vice 2300) was obtained and substituted into the modeled circuit. This completed, the frequency vs H parameter characteristics of the network were again obtained using ECAP. An extract of the results are given in Table six.

TABLE 6

f	h_{11}	h_{12}	h_{21}	h_{22}
1KHz	$45.2 \angle -167^\circ$	$1.0186 \angle -.001^\circ$	$1.000095 \angle 0^\circ$	$.295 \cdot 10^{-5} \angle 84^\circ$
1MHz	$47.6 \angle +172^\circ$	$1.0129 \angle -1.3^\circ$	$1.00008 \angle 0^\circ$	$.45 \cdot 10^{-5} \angle 72^\circ$

Having satisfied the $h_{12}h_{21}$ cross product requirement, it remained to eliminate the parasitics h_{11} and h_{22}. For the values of table six, an H parameter set of $h_{11} < 0$, $h_{22} \geq 0$, $h_{12}h_{21} > 1$, and $\Delta h < 0$ is noted. This equates to set 2b of table three. Thus, the desired compensation scheme was found to be equivalent to that shown in Figure 54.
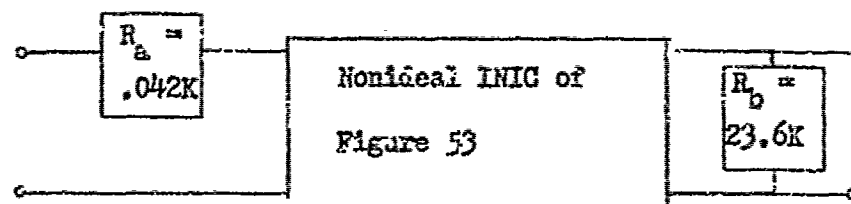

Fig. 54. Compensation for Nonideal INIC of Figure 53

The resultant frequency vs H parameter plots based on the output of the ECAP runs are shown in Figure 55 through 58.

Several factors were evident from the above data. First, h_{11} was too large at higher frequencies ($f > 100k$). This was corrected by modifying R_a to 45 and R_b to 37k. Secondly, one of the most important factors limiting high frequency performance was the presence of the collector-base capacitance of the two transistors, as expected, since both h_{21} and h_{22} actually contain jwC_1 terms of the form

$$h_{21} \approx \frac{R_2}{R_3}\left[\frac{1 - jwC_1R_3}{1 + jwC_1R_2}\right] \tag{40}$$

$$h_{22} \approx jwC_1\left[\frac{1 + R_2/R_3}{1 + jwC_1R_2}\right] \tag{41}$$

where C_1 is the lumped collector-base capacitance present. As the frequency of operation increases, it is apparent that h_{21} will approach a negative real number. This was partially overcome by placing a capacitance
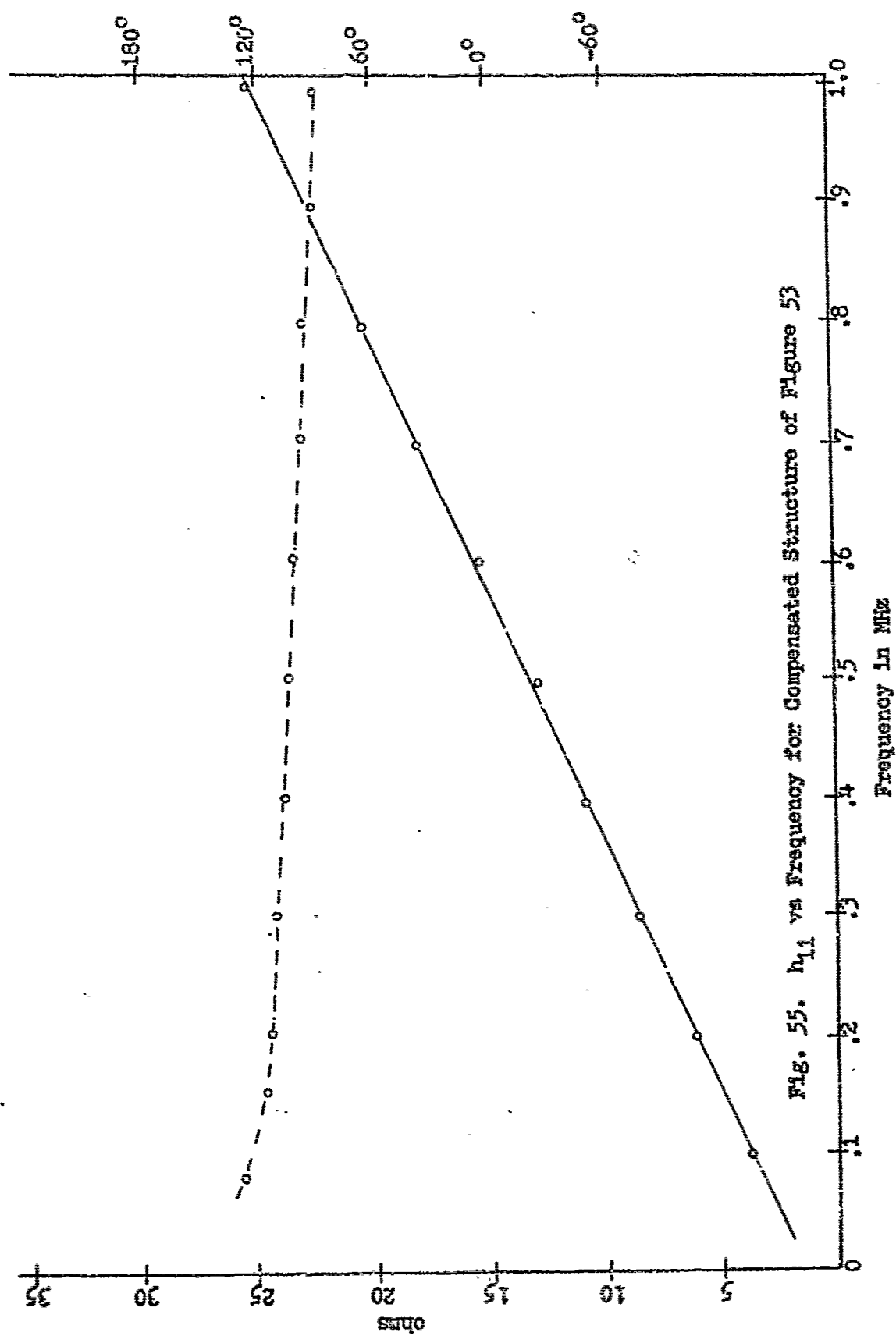
69

Fig. 55. h_{11} vs Frequency for Compensated Structure of Figure 53
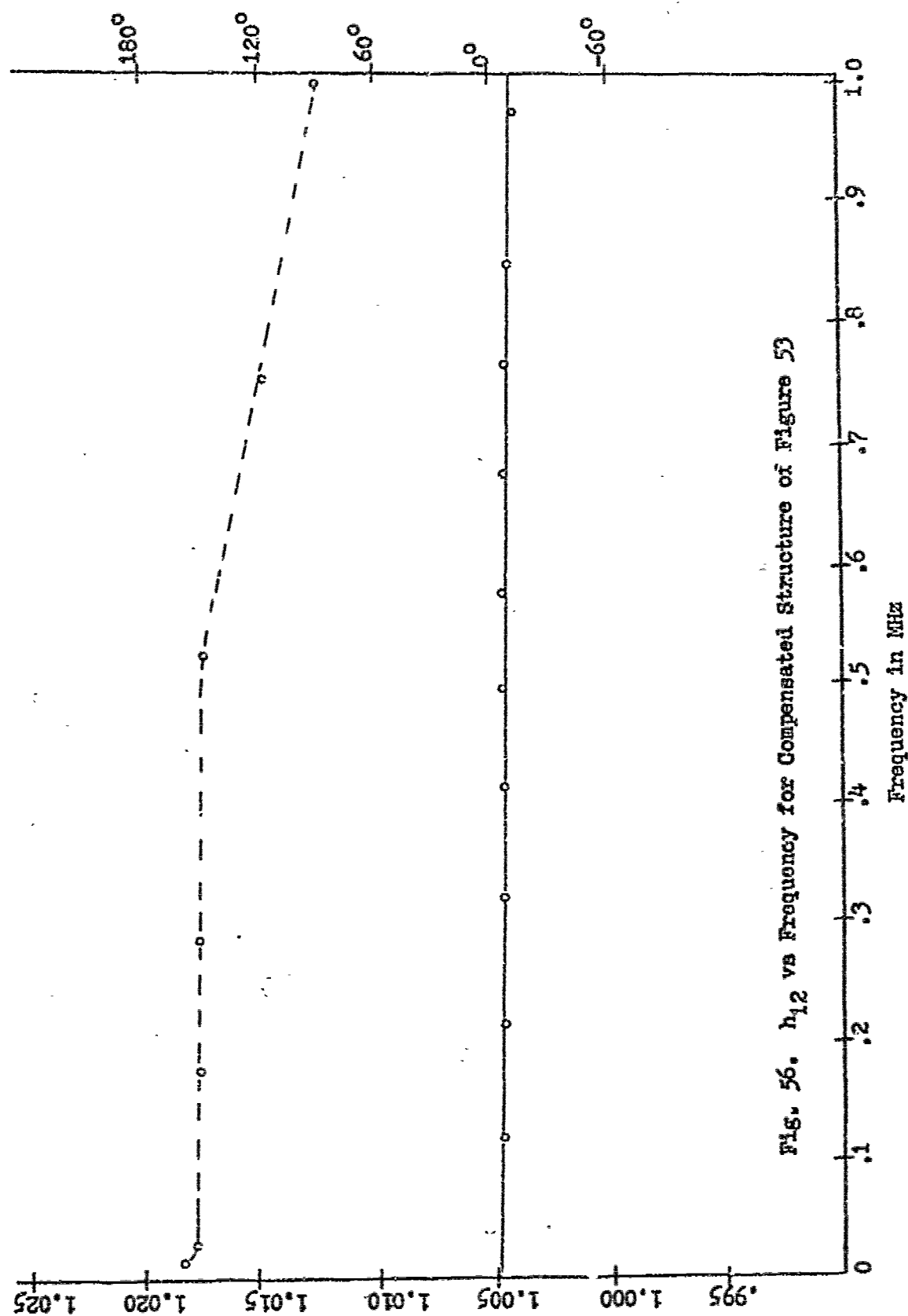
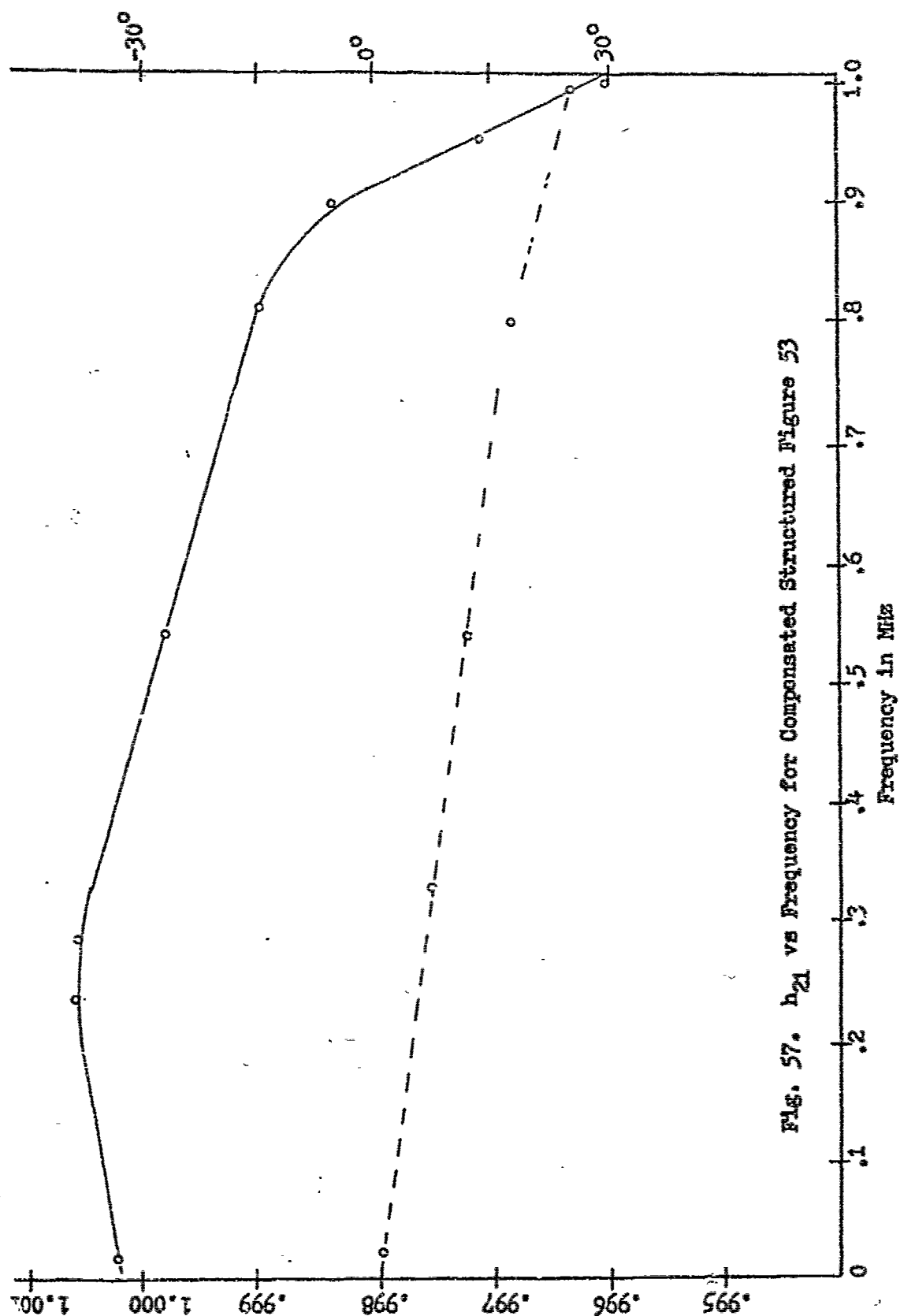Fig. 56. h_{12} vs Frequency for Compensated Structure of Figure 53

71

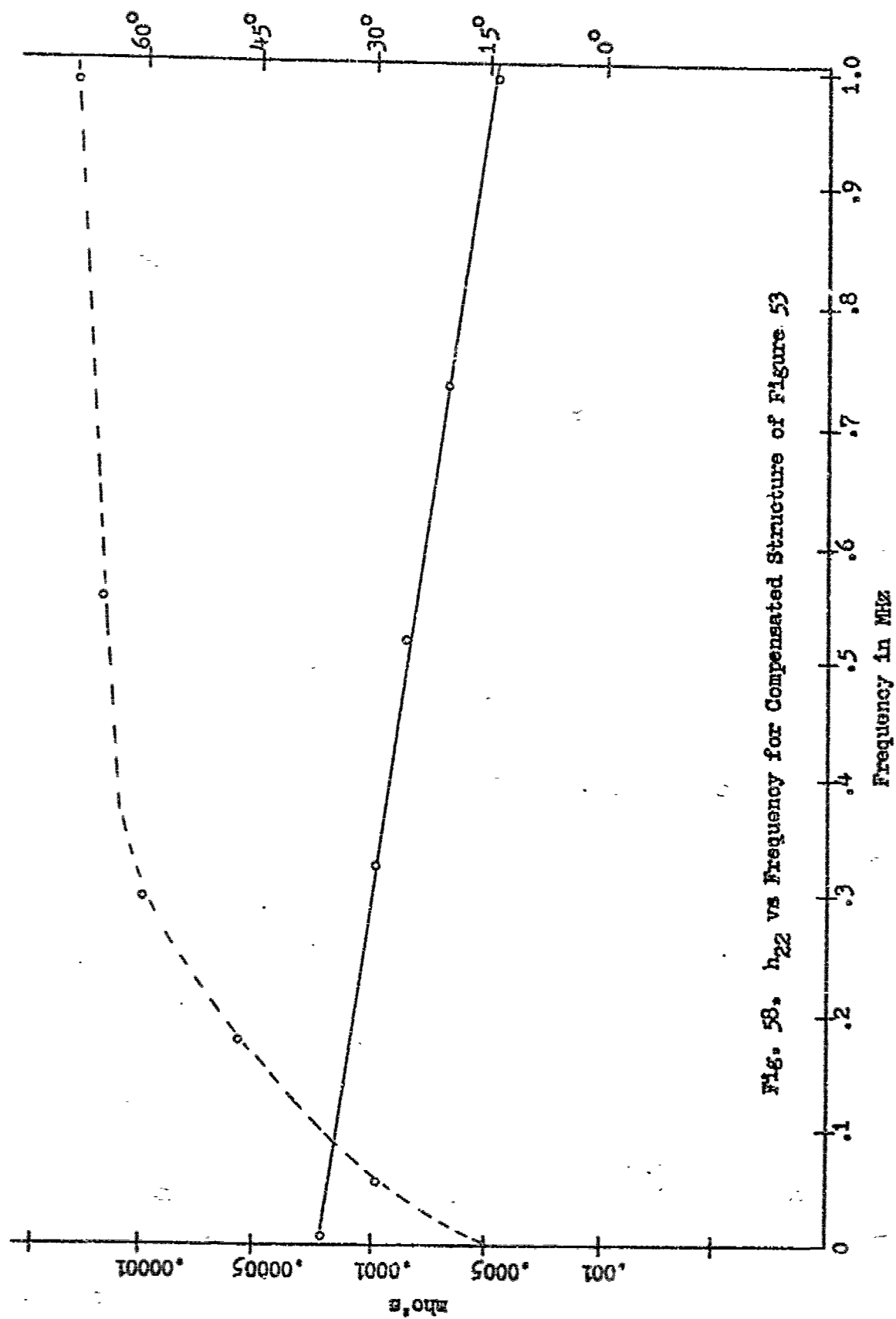Fig. 57. h_{21} vs Frequency for Compensated Structured Figure 53

Frequency in MHz

72

Fig. 58. h_{22} vs Frequency for Compensated Structure of Figure 53

73

C_2 in parallel with R_3. The effect of this was to modify the H parameters to

$$\begin{bmatrix} h_{11} = 0 & & b_{12} = 1 \\ \\ h_{21} = \dfrac{R_2}{R_3} \dfrac{1 + jw(C_2-C_1)R_3}{1 + jwC_2R_2} & & h_{22} = \dfrac{1 + R_2/R_3 + jwC_2R_1}{1 + jwC_1R_2} \end{bmatrix}$$

If in the above $R_2 = \text{p}$ and $C_2 = 2C_1$, then the above reduces to

$$\begin{bmatrix} h_{11} = 0 & h_{12} = 1 \\ \\ h_{21} = 1 & h_{22} = jwC_1 \end{bmatrix}$$

The only remaining departure from the ideal case left now is the non-zero value of h_{22}, which from consideration of table three, can be compensated by shunting a capacitance C_1 across the input. The above corrections were made, new circuit values inserted, and rerun for frequency vs H parameter characteristics. The results are summarized in table seven.

TABLE 7

f	h_{11}	h_{12}	h_{21}	h_{22}
1 KHz	$.4 \angle 179^\circ$	$1.005 \angle 163^\circ$	$1.0001 \angle 0$	$.5 \cdot 10^{-5} \angle 0$
10 KHz	$.9 \angle 134^\circ$	$1.005 \angle 161^\circ$	$1.001 \angle -2^\circ$	$.5 \cdot 10^{-5} \angle 7^\circ$
100 KHz	$1.6 \angle 119^\circ$	$1.0047 \angle 159^\circ$	$1.001 \angle -4^\circ$	$.6 \cdot 10^{-5} \angle 30^\circ$
1 MHz	$2.7 \angle 93^\circ$	$1.0043 \angle 82^\circ$	$1.0005 \angle -9^\circ$	$.6 \cdot 10^{-5} \angle 67^\circ$
10. MHz	$6.4 \angle 54^\circ$	$1.0041 \angle 71^\circ$	$1.0009 \angle -13^\circ$	$.9 \cdot 10^{-5} \angle 82^\circ$

The circuit was next tested using the HP 8405A Vector Voltmeter configuration of Figure 39. Using a 10K load, the results are summarized in table eight.

TABLE 8

Frequency	z_{in}/z_{load}
10 KHz	-.927 + j.0007
100 KHz	-.963 + j.0032
1 MHz	-.972 + j.006
10 MHz	-.961 + j.0013
20 MHz	-.943 + j.004

The above results were considered to be close enough to the anticipated values that no further circuit modifications were attempted. The final circuit form used in matching to the antenna loads is shown in Figure 59.
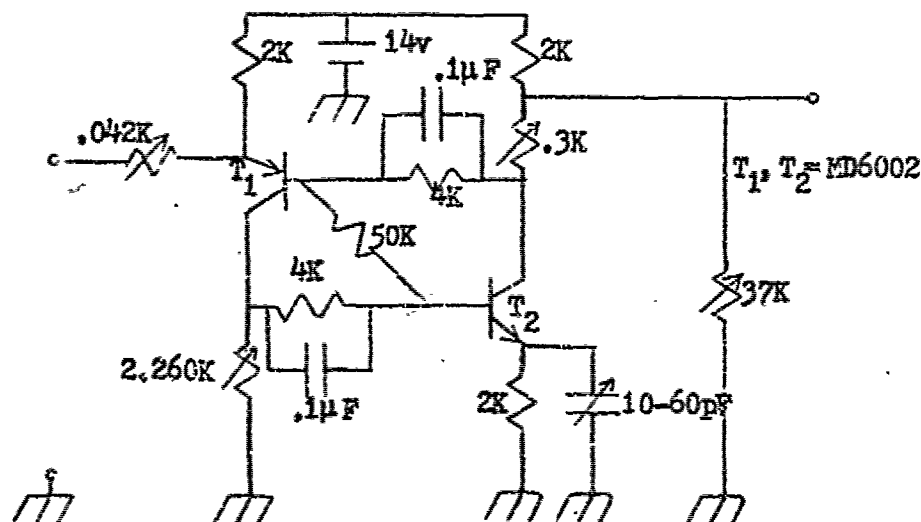

Fig. 59. Final Circuit Form of Nonideal INIC

The addition of the 50K resistance connecting the bases of the two transistors was found to be necessary if reliable transistor turn-on of both active devices were to be achieved.

2. Antenna Realizable Form

The circuit of Figure 59 was loaded with an antenna at each port, yielding the antenna structure of Figure 36b. Once again, a PRM-1A Radio Test Set and a 12 foot TRICOR whip were used to determine a figure of merit. The results of these tests are shown in Figure 60. The loss of gain above 1 MHz was attributed to the inability to exactly control the phase shift across the device, this in turn due to the complex nature of h_{21}, or equivalently, α.

Lastly, the previously mentioned comments concerning local broadcasting stations, peak signal into the circuit, and peak input into the test set, applied. The maximum signal that the circuit could handle was found to be approximately $\pm$ 2 volts, but since the PRM-1A was restricted to an input of $\pm$ .6 volts, it was of little importance.

C. NODAL ADMITTANCE MODEL

The last circuit model constructed was based on the nodal admittance synthesis procedure presented in chapter two.

1. Design Procedure

Using the circuit form of Figure 29, resistance values were selected to satisfy equations 19 through 21. The final circuit form is shown in Figure 61.[4]

---

[4] R_3 = 261 ohms for DC nulling. All power supplies shunted to ground with the parallel combination of .02 uF ceramic and 10 uF tantalum capacitors.

Fig. 60. Gain vs Frequency of Nonideal Synthesized Active Antenna System Relative to 12 foot Untuned Antenna

77
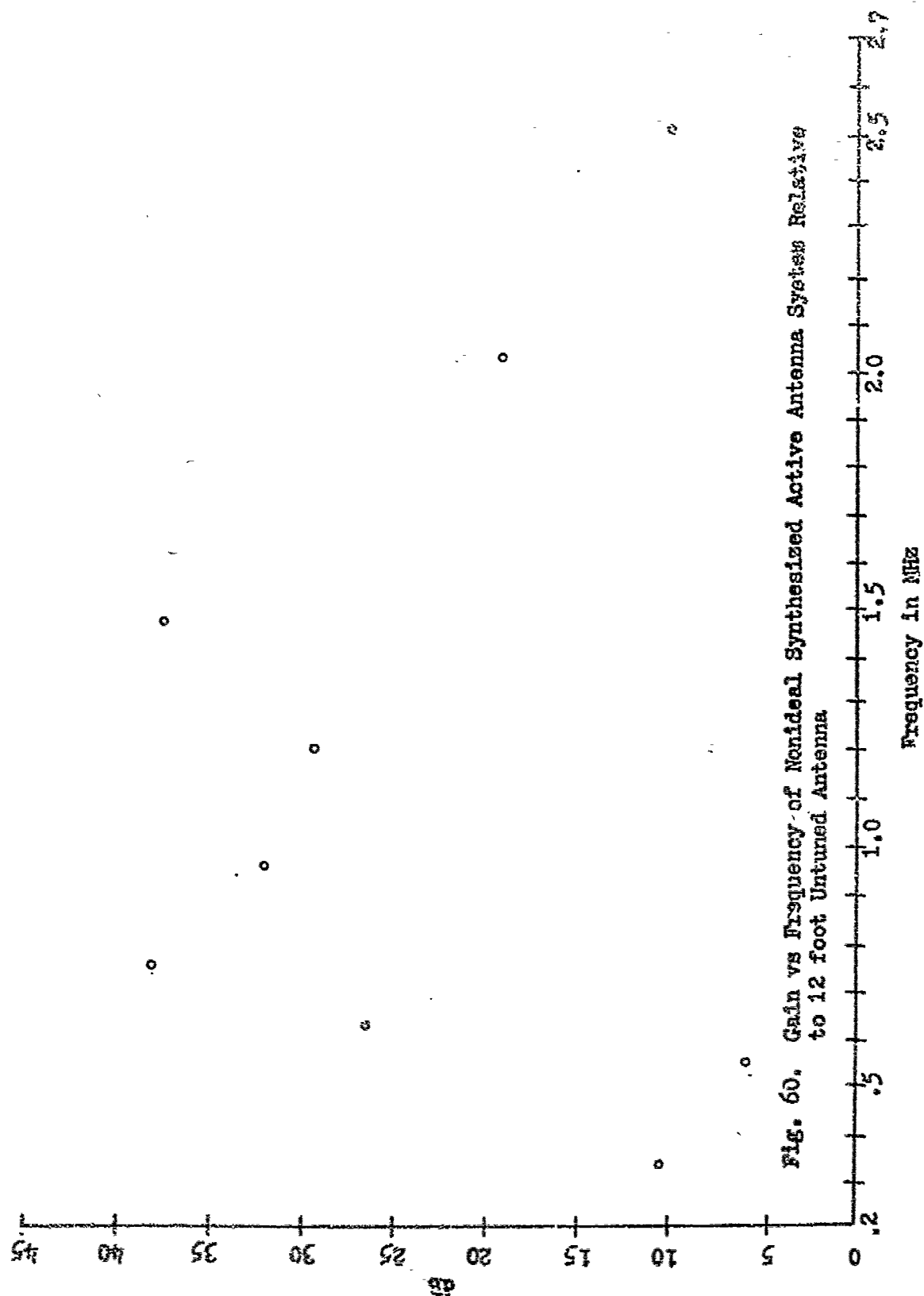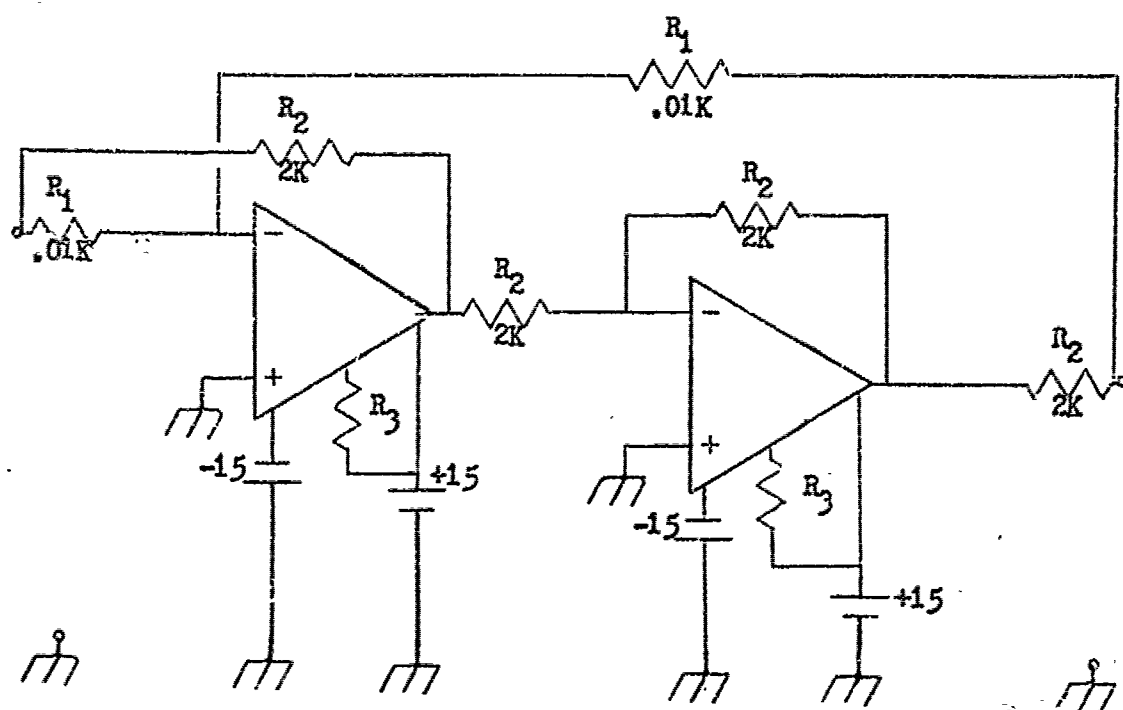
Fig. 61. Circuit Form of Nodal Admittance Model Constructed

This network was analyzed by using the G parameters, where for the ideal VNIC, G is given by:

$$[G] = \begin{bmatrix} 0 & -1 \\ -1 & 0 \end{bmatrix}$$

Using the circuit values given in Figure 61, the resultant G parameters were found to be:

$$\begin{bmatrix} g_{11} = \dfrac{2R_1}{A_{ol}} & g_{12} = -1 + \dfrac{2}{A_{ol}} \\ \\ g_{21} = -1 + \dfrac{2}{A_{ol}} & g_{22} = \dfrac{6}{R_2 A_{ol}} \end{bmatrix}$$

where it was assumed that the open-loop gain, A_{ol}, of each operational amplifier was identical and that associated input capacitances were negligible. Hence, for large values of A_{ol}, the matrix of equation 42 was satisfied.

2. Antenna Realizable Form

The circuit of Figure 61 was loaded at each port with top-loaded miniature antennaes, yielding once again the parallel conjugate antenna matching scheme of Figure 36b. Using the testing procedures previously discussed, the gain vs frequency characteristics relative to the untuned 12 foot TRICOR whip were obtained. This data is plotted in Figure 62.

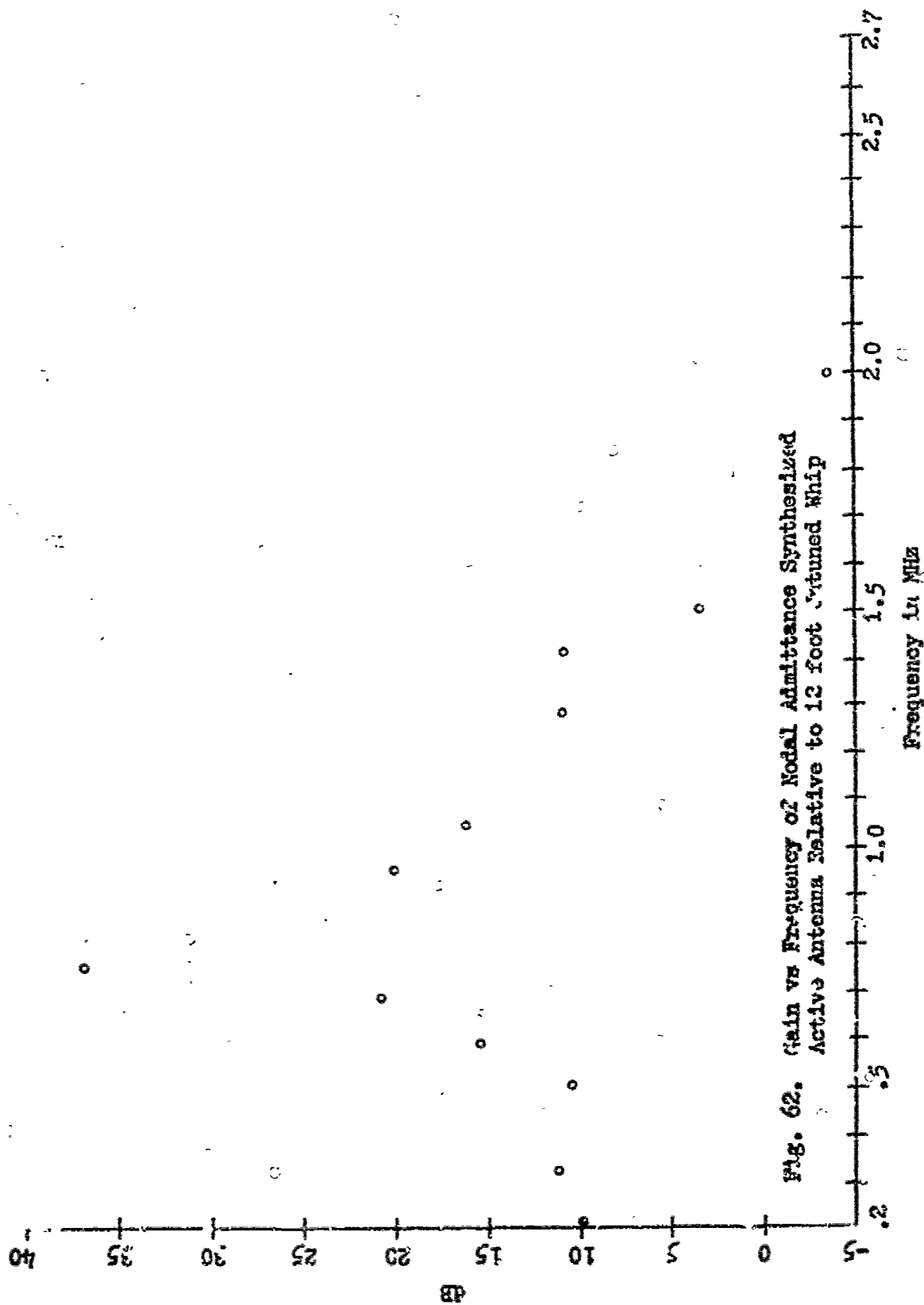Fig. 62. Gain vs Frequency of Nodal Admittance Synthesized
Active Antenna Relative to 12 foot detuned Whip

V. CONCLUSIONS

As has been pointed out, there are two aspects to the theory of conjugate antenna matching, the most critical of course being the actual achievement of the desired parameters for the active circuit utilized. When considering either the nonideal NIC or nodal admittance synthesized circuit realizations, it is evident that the devices are useful for only as long as the desired $[H]$ matrix parameters are obtained. In both of the above, the resulting phase shift across the device leads to the ultimate deterioration of the converter action above 20 MHz. As expected, the phase shift increases rapidly with frequency, and for the configuration of Figure 51, can be approximated by $\phi = 2\tan^{-1}w C_1 R_3$. This was observed experimentally under load conditions satisfying 100 ohms $< Z_1 <$ 10M.

It is generally accepted that NIC action can be achieved below 100 KHz without extensive compensation of the active network. Yet, above 100 KHz, as pointed out by equations 40 and 41, the conversion ratio K of the NIC will be a complex function of frequency. The effect of such nonideal converter action is drastic with respect to frequency limitations. Consider the transmission ratio K defined by

$$\frac{Z_{in}}{Z_{load}} = K = |h_{21}h_{12}| = a(w) + jb(w) \; ,$$

where $a(w)$ is a $\angle 1$, negative number. If, as with the small top loaded antenna, a reactive load is inserted,

$$Z_{in} = (a + jb) \; jY_L \; ,$$

$$Z_{in} = -bY_L + jaY_L \; ,$$

81

then the resultant impedance presented will lead to the presence of an unwanted, frequency dependent, real component. If it is assumed that some amount of impedance, Z_c, is added to compensate for the undesired real component; then

$$Z_{in} = (a + jb)(Z_c + jY_L) \quad ,$$

$$Z_{in} = (aZ_c - bY_L) + j(aY_L + bZ_c) \ .$$

If the real component is to equal zero, then $(aZ_c - bY_L)$ must equal zero. But, for this to be true over large frequency ranges, both $a(w)$ and $b(w)$ must change signs simultaneously. In general, due to the capacitance effect of the active devices, $b(w)$ cannot be controlled to the extent necessary if stability is to be maintained. This has been confirmed experimentally in numerous NIC circuit models. The final result, then, is two fold. First, a restriction of the useful high frequency range to the region in which the sign of $a(w)$ and $b(w)$ are identical and secondly, a deterioration of the converter action from the ideal case of $h_{21}h_{12} = 1$.

This last effect is more obvious if one considers the sensitivity values for the circuit of Figure 52. For this example,

$$Z_{in} = R_e + h_{11} - \frac{h_{12}h_{21}R_bZ_1}{R_b + Z_1 + h_{22}R_bZ_1}$$

and

$$S_{h_{11}}^{Z_{in}} \equiv \frac{dZ_{in}/Z_{in}}{dh_{11}/h_{11}} = \frac{-h_{11}}{Z_1} \quad ,$$

$$S_{h_{22}}^{Z_{in}} = \frac{dZ_{in}/Z_{in}}{dh_{22}/h_{22}} = -h_{22}Z_1 \quad ,$$

$$S_{h_{12}h_{21}}^{Z_{in}} \equiv \frac{dZ_{in}/Z_{in}}{d(h_{12}h_{21})/h_{12}h_{21}} = 1 \ .$$

It is evident from these relations that a variation in the gain

product $K = h_{12}h_{21}$ will have the greatest effect on NIC performance, es-

pecially if, as shown above, $h_{12}h_{21}$ is a complex function. In addition,

it was observed that h_{11} and h_{22}, the parasitic impedances, became im-

portant if either the load impedance was made very small or very large.

It would be expected that if the matrix modeled realizations were con-

structed on a stripline format, that higher frequencies of operation could

be obtained. For the time being, though, the main restriction would seem

to be the relatively low beta-cutoff frequencies of the present day tran-

sistors. What is required, in the most basic sense, is active devices

with f_t's > 20GHz, and extremely large β's.

With regard to the idealized generator model studied, it would appear

that the restrictions imposed by the above considerations would again be

detrimental. Though this is true, it is to a much lesser degree, since

the sensitivities involved are of a more favorable nature. In fact, the

principal degrading effect observed was due to the load impedance size

vice the presence of transmission phase shift.

It is to be noted that of the conjugate antenna systems constructed,

all were of a parallel form approximating Figure 36b. Though several

series placement arrangements were constructed, none were found to work

as well as the parallel configuration presented in this report. This was

primarily due to the inability to develop a NIC circuit with the proper

antenna-circuit-ground isolation required for proper converter action.

As a result, severe frequency range restrictions arose due to stability

restrictions.

Although none of the reviewed circuit/antenna arrangements were tested

exhaustively for stability and drift under variable operational conditions

and environment, it is apparent that the concept of conjugate antenna matching is feasible. It is to be emphasized that the matching accomplished in this report was done by tuning the active device once, and then testing for the gain vs frequency response, vice continual tuning. Hence, the shown frequency range of 100K to approximately 10-40 MHz still is impressive. However, though this is far short of a true broadband antenna system, it is evident that in the frequency range less than 30 MHz, the concept has considerable merit.

It is worthy of note, that it is possible to compensate the NIC-antenna system for the frequency dependence of α at frequencies greater than 30 MHz if the active device f_t is high enough. This, of course, is at the expense of sacrificing the usable frequency range. This approach was tested using the nonideal, discrete element circuit of Figure 57, and found to work satisfactorily at specific frequencies for which compensation was inserted.

The model was found to operate in the desired manner at 20 MHz, 40 MHz, and at a reduced level, due to atmospheric noise, of 50 MHz. A useful bandwidth of approximately 2-3 MHz was obtained with each of the compensation schemes used, this small amount of bandwidth due almost entirely to the rapid rate of phase shift across the device at those higher frequencies of operation.

It is anticipated that as substantial improvement in transistor high frequency technology occurs, that many of the above restrictions will be significantly reduced.

Thus, the final conclusion is that the concept is practical and capable of being implemented up to the lower VHF-range in a broadband manner, and that there exists now a significant means of reducing antenna size while realizing greater gain in the lower frequency regions.

APPENDIX A

Through the courtesy of Kollmorgen Corporation, a Kollmorgen model 848 Voltage Probe Antenna (VPA) was obtained for the purposes of making comparison tests against the active antenna system of Figure 41. Due to the fact that the above tests were conducted after the completion of the main text of this thesis, the results are contained herein.

The testing procedures employed were identical to those discussed on page 57 that led to Figures 43 and 44. The test results are presented in Figure 63, where gain over the VPA is plotted vs frequency.

Fig. 63. Gain vs Frequency of Active Antenna Radiated with Constant
Signal Source, Relative to Kollmorgen Model 848 VPA
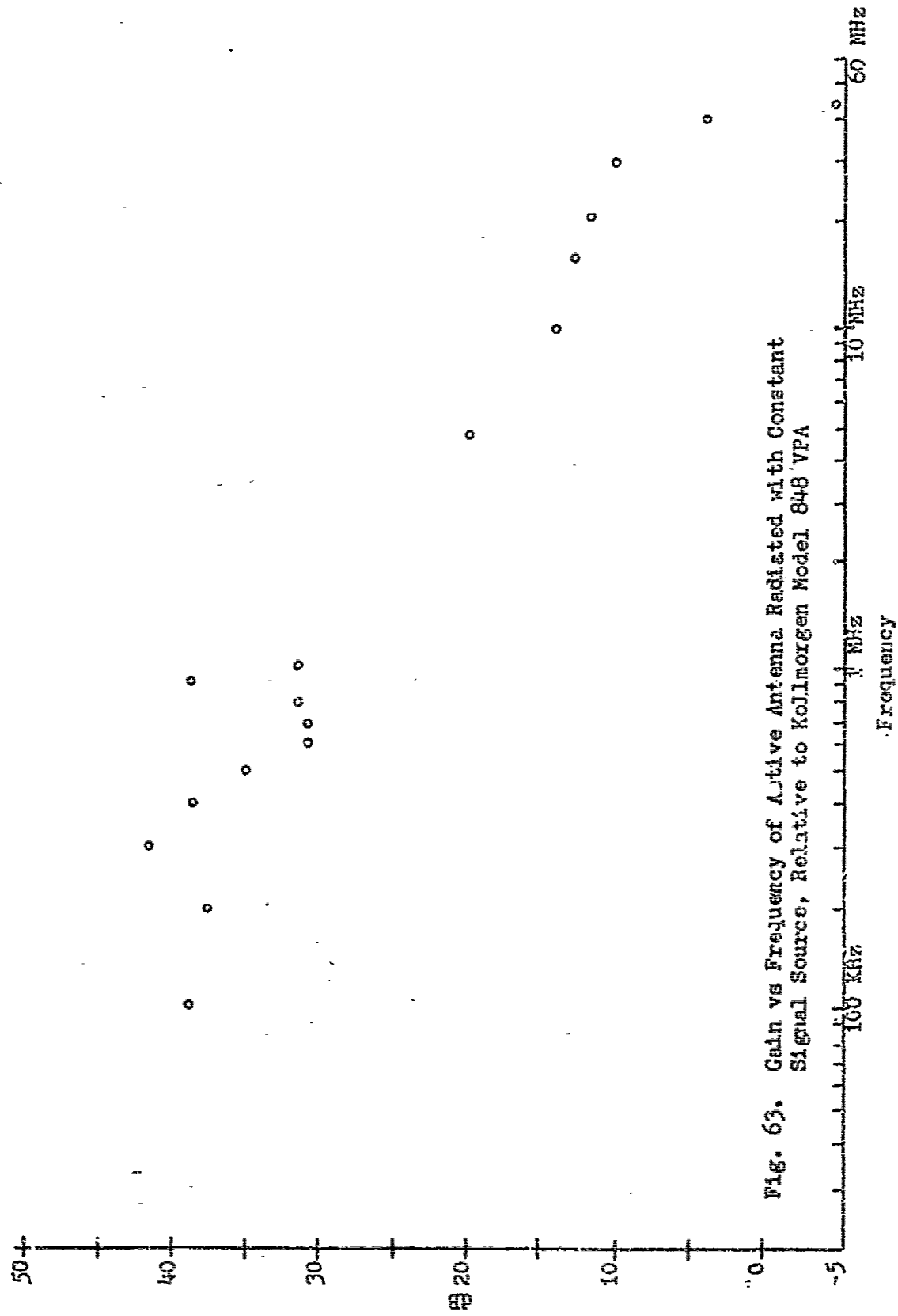
LIST OF REFERENCES

1. Carlin, H. J. and LaRosa, R., Proc. of the Symposium on Modern Synthesis, Polytech Inst. of Brooklyn, April 1952.

2. Fano, R.M., "Theoretical Limitations on the Broadband Matching of Arbitary Impedances," J. Franklin Inst., v. 249, p. 57, Jan. 1950 and p. 139, Feb. 1950.

3. Merrill, J.L. Jr., "Theory of Negative Impedance Converters," Bell Sys. Tech. J., v. 30, p. 88, 1951.

4. Bonner, A.L., Garrison, J.L., and Knopp, W.J.," The E-6 Negative Impedance Repeater," Bell Sys. Tech. J. Monogram 1382.

5. McMahon, E.L. and Liepa, V., "Techniques for Broadband Control of Radar Cross Sections," The University of Michigan Radiation Lab. Report No. 013630-8-T, AFCRL-71-0500.

6. University of Illinois Antenna Laboratory Technical Report No. 64, Antenna Impedance Matching by Means of Active Networks, by S. Laxpati and R. Mittra, AD No. 291766, Nov. 1962.

7. Harris, D.H., An Investigation of Broadband Miniature Antennas, M.S. Thesis, United States Naval Postgraduate School, Sept. 1968.

8. The ARRL Antenna Book, The American Radio Relay League, Inc., Newington, Conn., p. 63, 1960.

9. Mitra, S., Analysis and Synthe   s of Linear Active Networks, p. 32-68, Wiley, 1969.

10. Kuo, C.K. and Su, K.L., "Some New Four Terminal NIC Circuits," IEEE Transactions on Circuit Theory, p. 379-381, Aug. 1967.

11. Linvill, J.G., "Transistor Neg .ive Impedance Converters," Proc. IRE, v. 41, p. 725-729, June 1953.

12. Holt, A.J. and Carey, J. R., "Analog Circuits of Impedance Converters," IEEE Transactions on Circuit Theory, v. CT-15, p. 420, Dec. 1968.

13. Antoniou, A., "Negative Impedance Converters using Operational Amplifiers," Electronic Letters, v. 1, p. 88-89, June 1965.

14. Larky, A.I., "Negative Impedance Converters," IRE Transactions on Circuit Theory, v. CT-4, p. 124-131, Sept. 1957.

15. Brownlie, J.D., "On the Stability Properties of a Negative Impedance Converter," IRE Transactions on Circuit Theory, v. CT-13, p. 98, 1968.

16. Hoskins, R.F., "Stability of Negative Impedance Converters," Electronic Letters, v. 9, p. 341, Sept. 1966,

17. Kinariwala, B.K., "Synthesis of Active RC Networks," Bell Sys, Tech. J., v. 38, p. 1269, 1959.

18. Sipress, J.M., "Synthesis of Active RC Networks," IRE Transactions on Circuit Theory, v. CT-8, p. 260, 1961.

19. Rohrer, R.A., Active Network Matching of Arbitary Loads, Electronics Res. Lab., Univ. of Calif., Berkeley, Report No. 367, Series 60, June 1961.

20. Yanagisawa, T., "RC Active Networks Using Current Inversion Type Negative Impedance Converters," IRE Transactions on Circuit Theory, v. CT-4, p. 140, 1957.

21. Jensen, R.W. and Lieberman, M., IBM Electronic Circuit Analysis Program-Techniques and Applications, Prentice-Hall, 1968.

22. Drew, A.J. and Gorski-Popiel, "Directly-Coupled Negative Impedance Converters," Proc. IEE, London, v. 111, p. 1282, 1964.

23. Storey, D.J., and Cullyer, W.J., "Network Synthesis Using Negative Impedance Converters," Proc. IEE, London, v. 111, p. 891-906, 1964.